

**Sting Interference Effects on the Static,
Dynamic, and Base Pressure Measurements
of the Standard Dynamics Model Aircraft
at Mach Numbers 0.3 through 1.3**

**Fred B. Cyran
ARO, Inc.**

August 1981

Final Report for Period — June 1980 through December 1980

Approved for public release; distribution unlimited.

**ARNOLD ENGINEERING DEVELOPMENT CENTER
ARNOLD AIR FORCE STATION, TENNESSEE
AIR FORCE SYSTEMS COMMAND
UNITED STATES AIR FORCE**

NOTICES

When U. S. Government drawings, specifications, or other data are used for any purpose other than a definitely related Government procurement operation, the Government thereby incurs no responsibility nor any obligation whatsoever, and the fact that the Government may have formulated, furnished, or in any way supplied the said drawings, specifications, or other data, is not to be regarded by implication or otherwise, or in any manner licensing the holder or any other person or corporation, or conveying any rights or permission to manufacture, use, or sell any patented invention that may in any way be related thereto.

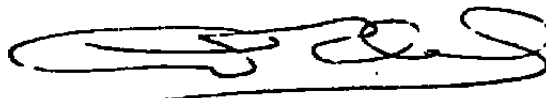
Qualified users may obtain copies of this report from the Defense Technical Information Center.

References to named commercial products in this report are not to be considered in any sense as an indorsement of the product by the United States Air Force or the Government.

This report has been reviewed by the Office of Public Affairs (PA) and is releasable to the National Technical Information Service (NTIS). At NTIS, it will be available to the general public, including foreign nations.

APPROVAL STATEMENT

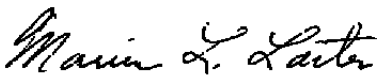
This report has been reviewed and approved.



ALVIN R. OBAL, Captain, CF
Directorate of Technology
Deputy for Operations

Approved for publication:

FOR THE COMMANDER



MARION L. LASTER
Director of Technology
Deputy for Operations

UNCLASSIFIED

REPORT DOCUMENTATION PAGE		READ INSTRUCTIONS BEFORE COMPLETING FORM
1 REPORT NUMBER AEDC-TR-81-3	2 GOVT ACCESSION NO.	3 RECIPIENT'S CATALOG NUMBER
4 TITLE (and Subtitle) STING INTERFERENCE EFFECTS ON THE STATIC, DYNAMIC, AND BASE PRESSURE MEASUREMENTS OF THE STANDARD DYNAMICS MODEL AIRCRAFT AT MACH NUMBERS 0.3 THROUGH 1.3		5 TYPE OF REPORT & PERIOD COVERED Final Report-June 1980 to December 1980
7. AUTHOR(s) Fred B. Cyran, ARO, Inc., a Sverdrup Corporation Company		6 PERFORMING ORG. REPORT NUMBER
9 PERFORMING ORGANIZATION NAME AND ADDRESS Arnold Engineering Development Center/DOT Air Force Systems Command Arnold Air Force Station, Tennessee 37389		10. PROGRAM ELEMENT, PROJECT, TASK AREA & WORK UNIT NUMBERS Program Element 65807F
11 CONTROLLING OFFICE NAME AND ADDRESS Arnold Engineering Development Center/DOS Air Force Systems Command Arnold Air Force Station, Tennessee 37389		12. REPORT DATE August 1981
14 MONITORING AGENCY NAME & ADDRESS (if different from Controlling Office)		13. NUMBER OF PAGES 64
		15. SECURITY CLASS (of this report) UNCLASSIFIED
		15a. DECLASSIFICATION/DOWNGRADING SCHEDULE N/A
16. DISTRIBUTION STATEMENT (of this Report) Approved for public release; distribution unlimited.		
17. DISTRIBUTION STATEMENT (of the abstract entered in Block 20, if different from Report)		
18. SUPPLEMENTARY NOTES Available in Defense Technical Information Center (DTIC)		
19. KEY WORDS (Continue on reverse side if necessary and identify by block number) wind tunnel tests subsonic pitch supports static stability yaw interference dynamic pressure angle of attack Mach number base pressure transonic derivatives (mathematics)		
20. ABSTRACT (Continue on reverse side if necessary and identify by block number) Wind tunnel tests were conducted in the Arnold Engineering Development Center (AEDC) Propulsion Wind Tunnel Facility (PWT) to provide sting-support interference information for planning and directing wind tunnel tests at subsonic and transonic Mach numbers. Sting length and diameter effects on static and dynamic stability derivatives, static pitching moments, and base pressure of the Standard Dynamics Model (SDM) were investigated at Mach numbers		

UNCLASSIFIED

20. ABSTRACT (Continued)

from 0.3 to 1.3. Dynamic stability derivatives were obtained at a nominal frequency of 5.2 Hz, at amplitudes of 1.0, 1.5, and 2.0 deg. Pitch and yaw data were both obtained as a function of angle of attack. Previously unpublished static force and moment data for the SDM are also presented.

The results showed that interference related to sting length was most pronounced at Mach number 0.95 for all measurements; the results also showed significant effects at Mach numbers 1.1 and 1.3 for yaw damping. Substantial sting diameter effects were observed at Mach number 0.3 for pitch damping and at Mach number 1.3 for yaw damping. Both sting length and diameter effects were found in base-pressure measurements at most Mach numbers.

PREFACE

The research reported herein was sponsored by the Arnold Engineering Development Center (AEDC), Air Force Systems Command (AFSC), Arnold Air Force Station, Tennessee. The results were obtained by ARO, Inc., AEDC Group (a Sverdrup Corporation Company), operating contractor for the AEDC. The work was done under ARO Project Numbers V32F-09A (D215VW) and P41C-H7. Captain Alvin R. Obal (CF) was the Air Force project manager. The manuscript was submitted for publication on December 29, 1980.

CONTENTS

	<u>Page</u>
1.0 INTRODUCTION	5
2.0 APPARATUS	
2.1 Test Facility	6
2.2 Test Article and Sting Hardware	6
2.3 Test Mechanism	7
2.4 Test Instrumentation	8
3.0 TEST DESCRIPTION	
3.1 Test Conditions and Procedures	9
3.2 Data Reduction	10
3.3 Uncertainty of Measurements	10
4.0 RESULTS AND DISCUSSION	
4.1 Sting Interference as a Function of Angle of Attack	11
4.2 Sting Length Effects at $\alpha = 0$	12
4.3 Combinations of Sting Length and Sting Diameter Interference Effects at $\alpha = 0$	13
5.0 CONCLUDING REMARKS	15
REFERENCES	18

ILLUSTRATIONS

Figure

1. Standard Dynamics Model (SDM) Details	21
2. Photograph of Model Installation in Aerodynamic Wind Tunnel (4T)	22
3. Details of Model Support Configurations, $d_s/d = 0.40$	23
4. Details of Model Support Configurations, $d_s/d = 0.65$ and 0.73	24
5. Details and Photograph of VKF 1.C Forced-Oscillation Test Mechanism	25
6. Variation of Pitching Moment with Sting Length as a Function of Angle of Attack	26
7. Typical Variation of Pitching-Moment Slope with Sting Length as a Function of Angle of Attack	27
8. Variation of Yawing-Moment Slope with Sting Length as a Function of Angle of Attack	28
9. Variation of Pitch-Damping Derivatives with Sting Length as a Function of Angle of Attack	29

<u>Figure</u>	<u>Page</u>
10. Variation of Yaw-Damping Derivatives with Sting Length as a Function of Angle of Attack	30
11. Variation of Base Pressure Ratio with Sting Length as a Function of Angle of Attack	31
12. Variation of Pitching-Moment Slope with Sting Length for Various Sting Diameters	32
13. Variation of Yawing-Moment Slope with Sting Length for Various Sting Diameters	33
14. Variation of Pitch-Damping Derivatives with Sting Length for Various Sting Diameters	34
15. Variation of Yaw-Damping Derivatives with Sting Length for Various Sting Diameters	35
16. Variation of Base Pressure Ratio with Sting Length for Various Sting Diameters	36

TABLES

1. Standard Dynamics Model (SDM) Dimensions	37
2. Standard Dynamics Model (SDM) Configuration Codes	38
3. Test Conditions	39
4. Test Summary	40
5. Estimated Uncertainties	46

APPENDIX

AERODYNAMIC CHARACTERISTICS OF THE SDM	53
NOMENCLATURE	62

1.0 INTRODUCTION

Within the last few years, the demand for more accurate wind tunnel data has placed greater emphasis on the evaluation of sting-support interference effects. Often, an aerodynamicist must understand support interference to accurately predict full-scale flight vehicle characteristics based on wind tunnel data. To obtain information on the evaluation of support interference effects, a continuing research program was initiated at the Arnold Engineering Development Center (AEDC) von Kármán Gas Dynamics Facility (VKF) in 1976; the results of various previous tests supporting this research program are documented in Refs. 1 through 4. Briefly, the history of this research program may be summarized as follows:

1. 1976 — investigated the effects of support interference on dynamic stability and base-pressure measurements of a 7-deg cone at Mach number 3 (Ref. 1);
2. 1977, 1978 — extended the Mach range of previous work to span the Mach 2-to 8-range and investigated interference effects on both base- and surface-pressure measurements of a 6-deg sliced-base cone (Ref. 2);
3. 1979 — concluded the investigation of support interference effects on the 7-deg cone by extending the previous range to encompass subsonic and transonic Mach numbers (Refs. 3 and 4).

The present work extends the 1979 research in the subsonic-transonic region to include the testing of a typical aircraft configuration. Future programs are planned at AEDC to extend the present research to the testing of a typical missile configuration.

The primary objective of the 1980 research was to define critical sting lengths for a typical aircraft configuration in subsonic and transonic flow. Critical sting length is generally defined as the shortest sting length that does not change the level of an aerodynamic measurement obtained with longer stings. In this report the critical sting lengths are defined by the measurements of pitch-damping derivatives, yaw-damping derivatives, pitching moment slope, yawing moment slope, static pitching moment, and base pressure. A secondary objective was to investigate the influence of sting diameter interference effects.

The test model was the Standard Dynamics Model (SDM). The forced-oscillation technique was used to obtain data at model oscillation amplitudes of 1.0, 1.5, and 2.0 deg. The frequency of oscillation was nominally 5.2 Hz. Data were obtained at angles of attack

from -6 to 25 deg at Mach numbers 0.3 to 1.3. The effective sting length was varied from 1 to 6 model diameters by positioning a conical flare at various stations along the sting for sting diameters of 0.40, 0.65, and 0.73 model diameters. The Reynolds number per foot ranged from 0.5×10^6 to 5.0×10^6 , and the reduced frequency parameter ($\omega d/2V$) varied from 0.009 to 0.032. The test was conducted in the Propulsion Wind Tunnel Facility (PWT), Aerodynamic Wind Tunnel (4T) from June 2 — 10, 1980 (pitch phase), and from September 6 — 10, 1980 (yaw phase). The test data in this report are also documented in Ref. 5.

This report will focus primarily on the effects of sting interference on the SDM. In addition, the basic aerodynamic characteristics of the SDM are presented in the Appendix. These characteristics were obtained both during the present interference investigation and from previously unpublished data obtained at AEDC.

Although an analysis of sting interference effects at subsonic and transonic Mach numbers on general model configurations is beyond the scope of this report, the results of this report should be applicable to similar aircraft and wing configurations mounted on similar sting supports. For further information on support interference in general, the reader is referred to the extensive bibliography of Ref. 2.

2.0 APPARATUS

2.1 TEST FACILITY

The Aerodynamic Wind Tunnel (4T) is a closed-loop, continuous-flow, variable-density tunnel in which the Mach number can be varied from 0.1 to 1.3 and can be set at discrete Mach numbers of 1.6 and 2.0 by placing nozzle inserts over the permanent sonic nozzle. Stagnation pressure can be varied from 400 to 3,400 psfa at all Mach numbers. The test section is 4 ft square and 12.5 ft long with perforated, variable-porosity (0.5-to 10-percent open) walls. It is completely enclosed in a plenum chamber from which the air can be evacuated, allowing part of the tunnel airflow to be removed through the perforated walls of the test section. The model support system consists of a sector and boom attachment which has a pitch angle capability of -7.5 to 28 deg with respect to the tunnel centerline and a roll capability of -180 to 180 deg about the sting centerline. Reference 6 gives a more complete description of the tunnel.

2.2 TEST ARTICLE AND STING HARDWARE

The Standard Dynamics Model (SDM) represents a 1/18-scale fighter-type aircraft. Basic details of the SDM are shown in Fig. 1, and pertinent dimensions are listed in Table 1. The

model has a 19.8-in. wing span and double-taper leading and trailing edges on the wing, stabilators, and vertical tail. The stabilators may be deflected in increments of ± 5 deg. All external components (i.e., wings, stabilators, inlet, ventral fins, canopy, and so forth) may be removed for buildup testing as desired. The model base diameter (d) is 4.375 in. The model was constructed of stainless steel, aluminum, and Densiloy[®]; both design and fabrication were performed at AEDC.

Table 2 lists and describes the SDM configurations tested during this investigation. Additional information, including complete details of the various SDM components, may be found in Ref. 5.

Figure 2 shows a photograph of a typical model-sting configuration installed in Tunnel 4T. The sting configuration shown in Fig. 2 is the "baseline" or minimal interference configuration, with the longest effective sting length (ℓ) and smallest sting diameter (d_s). For the smallest sting diameter configuration ($d_s/d = 0.40$), the effective sting length was shortened by positioning a conical steel flare (Fig. 3) at stations 2.0, 3.0, 4.0, 5.0, 5.6, and 5.7 model diameters to the rear of the model base along the sting. Without the conical steel flare installed, the effective sting length was 6.0 model diameters. The flare was mounted to the motor housing of the test mechanism and did not come in contact with the sting forward of the motor housing.

For the larger sting diameter configurations ($d_s/d = 0.65$ and 0.73) (Fig. 4), the steel conical flare was positioned fully aft of the model (against the motor housing as shown in Fig. 3b). Two different sets of split tubes were mounted to the front end of this flare. The tubes were designed to split into halves to facilitate installation without removing the model. The split tubes were installed such that their parting line was in the vertical plane. The effective sting length was shortened by positioning a Lexan[®] flare on the split tubes 1.0, 2.0, 3.0 and 4.0 model diameters to the rear of the model base along the sting. Without the Lexan flare, the effective sting length was 5.6 model diameters. No part of the sting diameter hardware touched the sting forward of the motor housing although the sting was subject to static and dynamic deflections within the tubes.

2.3 TEST MECHANISM

The VKF 1.C Forced-Oscillation Test Mechanism (Fig. 5) utilizes a cross-flexure pivot, an electric shaker motor, and a one-component moment beam which is instrumented with strain gages to measure the forcing moment of the shaker motor. The motor is coupled to the moment beam by means of a connecting rod and flexural linkage which converts the translational force to a moment to oscillate the model at amplitudes up to 3 deg (depending

on flexure balance) and frequencies from 2 to 8 Hz. The cross flexures, which are instrumented to measure the pitch or yaw displacement, support the model loads and provide the restoring moment to cancel the inertial moment when the system is operating at its natural frequency. The moment beam is not subjected to the static loads and can be made as sensitive as required for the dynamic measurements.

Data from this test were obtained with the 0.180-in.-thick cross flexures, which have a stiffness of 962.5 ft-lb/radian. The moment beam used to measure the pitch-damping moments was 0.047-in. thick and was designed for a maximum moment of 11.3 in.-lb. For measuring the yaw-damping moments, the moment beam was 0.036 in. thick and was designed for a maximum moment of 7.1 in.-lb.

The cross-flexure pivot, moment beam, and flexural linkage assembly, are supported by a long, slender cylindrical sting with a 1-deg taper. The sting is instrumented with strain gages to measure the static and oscillatory deflections of the sting in both the pitch and yaw plane. A pneumatic- and spring-operated locking device is provided on the balance to hold the model during tunnel startup and shutdown.

2.4 TEST INSTRUMENTATION

2.4.1 Forced-Oscillation Instrumentation

The forced-oscillation instrumentation (Ref. 7) uses an electronic analog system with precision electronics. The control, monitor, and data acquisition instrumentation are contained in a portable console that can be interfaced easily with the instrumentation of the various wind tunnels at AEDC. The control instrumentation provides a system that can vary the oscillation amplitude of the model within the flexure limits. An electronic feedback loop controls the oscillation amplitude, thereby permitting testing of both dynamically stable and unstable configurations. Data are normally obtained at or near the natural frequency of the model flexure system; however, the electronic resolvers permit data to be obtained off resonance.

All gages are excited by d-c voltages, and outputs are increased to optimum values by d-c amplifiers. Typical balance outputs from an oscillating model are composed of oscillatory components (OC) superimposed on static components (SC). These components are separated by band-pass and low-pass filters. The SC outputs are used to calculate the static moment coefficients and static sting deflections. The OC outputs are input to the resolver instrumentation and precise frequency measuring instrumentation. The resolvers utilize very accurate analog electronic devices to process the OC signals and output d-c voltages. The

output d-c voltages are proportional to the amplitude squared, the in-phase and quadrature (90-deg out-of-phase) balance components (forcing torque), and the in-phase and quadrature sting components. An analog-to-digital (A/D) converter converts these outputs to digital signals. The data are recorded for a designated period of time ranging from approximately 2 to 60 sec at a sample rate appropriate for the type of test and wind tunnel.

2.4.2 Model Base Pressure Instrumentation

Model base pressure was measured with two pressure transducers located on the tunnel plenum chamber wall. The base pressure orifices (0.062 in. ID) were located on the surface of the sting at the model base plane.

3.0 TEST DESCRIPTION

3.1 TEST CONDITIONS AND PROCEDURES

3.1.1 General

Table 3 summarizes the nominal test conditions at each Mach number, and Table 4 gives the test summary. The reduced frequency parameter ($\omega d/2V$) ranged from 0.009 radians at Mach 1.3 to 0.032 radians at Mach 0.3. The nominal oscillation frequency was 5.2 Hz. Most of the data were obtained at an oscillation amplitude of 1.0 deg, but amplitudes of 1.5 and 2.0 deg were also used for selected conditions.

The test was conducted in two phases: the pitch phase (June 2 — 10, 1980) and the yaw phase (September 6 — 10, 1980). Testing procedures for the yaw phase were identical to those for the pitch phase, except that the test mechanism was rolled +90 deg from the pitch plane to the yaw plane. In addition, guy-rod stiffeners were attached to the sector and boom assembly to help dampen vibration of the boom in yaw during the yaw phase.

3.1.2 Data Acquisition

After tunnel conditions and model attitude were established, the model was unlocked and brought to a constant oscillation amplitude of 1.0, 1.5, or 2.0 deg by use of the Forced-Oscillation Control System. The system was allowed to stabilize at the system resonant frequency before the data (including base pressure) were recorded. Data were obtained over a 30-sec time interval at each data point. The balance and sting gage outputs and the frequency instrumentation outputs were read from the forced-oscillation instrumentation console by a Digital Data Acquisition System (DDAS), at a rate of approximately 200 samples per second.

The Automatic Model Attitude Positioning System (AMAPS) controlled the model position. The model angle-of-attack requirements were programmed into the AMAPS prior to the test. After data were obtained at a given angle of attack, the AMAPS was manually activated, and the model was automatically pitched to the next required angle of attack.

3.2 DATA REDUCTION

Data from the DDAS were combined with tunnel model attitude and base pressure instrumentation data and sent directly to a DEC-10 System computer. Average values of the balance and sting gage outputs were calculated by the computer and were used in conjunction with the remaining DDAS outputs to calculate the dynamic derivatives. Both the SC and OC sting gage outputs were used to correct the data for sting bending effects. The data reduction method is given in Refs. 7 and 8.

3.3 UNCERTAINTY OF MEASUREMENTS

In general, instrumentation calibrations and data uncertainty estimates were made using methods recognized by the National Bureau of Standards (NBS) (Ref. 9). Measurement uncertainty is a combination of bias and precision errors defined as

$$U = \pm (B + t_{95}S)$$

where B is the bias limit, S is the sample standard deviation, and t_{95} is the 95th percentile point for the two-tailed Students "t" distribution, which equals 2 for degrees of freedom greater than 30.

Estimates of the measured data uncertainties for this test are given in Tables 5a and b. The balance data uncertainties were determined from in-place static and dynamic calibrations made through the data recording system and data reduction program. Static load hangings on the balance and sting simulate the range of loads anticipated during the test, and measurement errors are based on differences between applied loads and corresponding values calculated from the equations used in the data reduction. Load hangings to verify the balance calibrations were made in place on a special calibration model. Uncertainties in the measurements of sting effects were included in the error analysis. To evaluate the still-air damping contribution, structural damping values were obtained at near-vacuum conditions before the tunnel flow was started.

Propagation of the bias and precision errors of measured data through the calculated data was made in accordance with Ref. 9; the results are given in Table 5c. The uncertainties

are for steady-state conditions. Occasionally, vibration and noise of the wind tunnel environment caused the scatter in the data to exceed the estimated uncertainty.

4.0 RESULTS AND DISCUSSION

The Appendix should be consulted for prefatory information on the static and dynamic characteristics of the model. The characteristics presented include C_N , C_A , C_t , C_m , C_Y , C_n , C_{m_α} , $C_{n_\beta} \cos \alpha$, $C_{m_\alpha} + C_{m_\alpha}$, $C_{n_\beta} - C_{n_\beta} \cos \alpha$, and base-pressure data as functions of angle of attack and Mach number, obtained from the present test and other sources. The Appendix also presents (1) comparison plots of C_m and C_{m_α} obtained from different wind tunnel tests to establish the validity of the present data, (2) effects of Reynolds number on static and dynamic derivatives and base pressure, and (3) effects of oscillation amplitude on pitch- and yaw-damping derivatives.

Results and discussions of particular aspects of the sting interference investigation on the SDM are presented as follows: Section 4.1 discusses the effects of sting length as a function of angle of attack, and is divided into subsections pertaining to these effects on specific measurements. Next, Sec. 4.2 discusses the use of sting length interference data obtained at zero angle of attack to represent sting length interference over the angle-of-attack range. Finally, Sec. 4.3 discusses the combined interference effects of sting length and diameter at zero angle of attack, and is also subdivided into subsections pertaining to specific measurements. Unless otherwise noted, all lines faired through the data presented in this section correspond to either the largest l/d or smallest d/d (the minimal interference data) which was tested.

4.1 STING INTERFERENCE AS A FUNCTION OF ANGLE OF ATTACK

Presented in this section are the effects of sting length interference on static and dynamic parameters as a function of angle of attack. Sting diameter effects were investigated at zero angle of attack and will be presented later. All results in this section are based on the data obtained with the smallest sting diameter ($d/d = 0.40$).

4.1.1 C_m Measurements

Figure 6a shows a typical variation of C_m with sting length as a function of angle of attack. This plot is representative of the interference effects at other Mach numbers in that, generally, no sting length effects were found over the angle-of-attack range investigated. An exception to this is the data for Mach number 0.95, for which decreasing effective sting length produced a slight, destabilizing effect at the higher angles of attack (Fig. 6b).

4.1.2 $C_{m\alpha}$ Measurements

Figure 7a shows a typical variation of $C_{m\alpha}$ with sting length as a function of angle of attack. Essentially no effects of sting length on $C_{m\alpha}$ were found at any substantial angle of attack although slight effects were observed at zero angle of attack at Mach number 0.95. These slight effects are shown in Fig. 7b and are discussed in more detail in Sec. 4.3.1.

4.1.3 $C_{n\beta} \cos \alpha$ Measurements

Typical sting length interference effects on the measurement of $C_{n\beta} \cos \alpha$ as a function of angle of attack are shown in Fig. 8a. In general, no interference effects were found, with two exceptions at Mach numbers 1.10 and 0.95. The Mach 1.10 data revealed significant interference effects at $\alpha = 0$, as shown in Fig. 8b. The slight interference effects again noted at Mach 0.95 at $\alpha = 0$ are discussed in Sec. 4.1.4.

4.1.4 $C_{m_q} + C_{m\alpha}$ Measurement

Figure 9a shows a typical variation of $C_{m_q} + C_{m\alpha}$ with sting length as a function of angle of attack. This figure is typical of the negligible effects of sting length found at all Mach numbers tested except for Mach number 0.95. The data obtained at $M = 0.95$ (Fig. 9b) indicated that interference is dynamically destabilizing at all angles of attack (from -4 to 14 deg) although it is most pronounced in the 0- to 8-deg range.

4.1.5 $C_{n_r} - C_{n\beta} \cos \alpha$ Measurement

Essentially no interference effects were found at Mach number 0.6 at all angles of attack. Data at $M = 1.3$ (Fig. 10a) showed a slight effect only at $\alpha = 0$. Interference at $M = 0.95$ and 1.10 (Figs. 10b and 10c, respectively) showed a substantially larger influence at $\alpha = 0$ than did the $M = 1.3$ data, with the interference diminishing with increasing angle of attack. No effects were found at $M = 0.95$ for $\alpha \geq 8$ deg. In all cases, the interference effects increased the magnitude of $C_{n_r} - C_{n\beta} \cos \alpha$ (increased dynamic stability).

4.1.6 p_b/p Measurement

With the exception of the data obtained at $M = 1.3$, the level of sting length interference on p_b/p was virtually constant at all angles of attack, as the typical plot in Fig. 11a shows. At $M = 1.3$ (Fig. 11b), interference gradually decreased from a maximum at $\alpha = 0$ to no effect at $\alpha = 14$ deg. At all Mach numbers, the interference effect increased the base-pressure ratio.

4.2 STING LENGTH EFFECTS AT $\alpha = 0$

The preceding summaries of data showed that for all measurements investigated, sting length interference effects usually peaked in the neighborhood of $\alpha = 0$. Generally, the interference effects gradually decreased as angle of attack increased. Thus, the definition of critical sting length based solely on data at $\alpha = 0$ is representative of sting length interference at angles of attack in the range from -4 to 14 deg (and possibly higher). However, at angles of attack *other* than zero, this value of critical sting length may be significantly conservative. The influence of sting diameter effects combined with sting length effects must be considered before any conclusions can be made about critical sting length. Both of these effects and the definition of critical sting length for various measurements and Mach numbers will be discussed in Section 4.3.

A limited investigation of oscillation amplitude effect on critical sting length determined by the measurement of $C_{m_q} + C_{m_\alpha}$ was conducted at Mach numbers 0.30, 0.60, 0.95, 1.10, and 1.30 at $\alpha = 0$ with the smallest sting diameter. Although the magnitude of $C_{m_q} + C_{m_\alpha}$ changed as a function of amplitude at some Mach numbers, a critical sting length dependence on amplitude was not found (only amplitudes of $\theta = 1$ and 2 deg were tested).

4.3 COMBINATIONS OF STING LENGTH AND DIAMETER INTERFERENCE EFFECTS AT $\alpha = 0$

The variations of the parameters C_{m_α} , $C_{n_\beta} \cos \alpha$, $C_{m_q} + C_{m_\alpha}$, $C_{n_r} - C_{n_\beta} \cos \alpha$, and p_b/p with effective sting length ratio (ℓ_s/d) are shown in Figs. 12 through 16 for several sting diameter ratios (d_s/d). Each parameter will be discussed.

4.3.1 C_{m_α} Measurement

Figure 12 indicates that for the range of sting diameters tested, C_{m_α} is largely independent of sting diameter at all Mach numbers and shows a slight dependency on sting length at $M = 0.95$. Sting length interference effects at $M = 0.95$ were characterized by a decrease in static pitch stability (increased C_{m_α}). From the faired lines in Fig. 12, the critical sting length ratio (ℓ_{cr}/d) is defined at $M = 0.95$ as equal to an ℓ_s/d of 3, and ℓ_{cr}/d is undefined at the other Mach numbers. For Mach numbers other than 0.95, it can be concluded from Fig. 12 that either $\ell_{cr}/d \leq 2$ or that C_{m_α} is independent of ℓ_s/d .

4.3.2 $C_{n_\beta} \cos \alpha$ Measurement

The effects of both sting length and diameter on $C_{n_\beta} \cos \alpha$ are shown in Fig. 13. At $M = 0.95$, sting length effects caused a decrease in $C_{n_\beta} \cos \alpha$, with a resulting ℓ_{cr}/d of 2. Also,

sting diameter effects at Mach number 0.95 were essentially negligible for the range of sting diameters tested. No conclusions can be drawn at $M = 0.3$ because of insufficient data. No effect of sting length or sting length or diameter was found in $C_{n\beta} \cos \alpha$ at any other Mach numbers.

4.3.3 $C_{m_q} + C_{m_\alpha}$ Measurement

Interference effects on $C_{m_q} + C_{m_\alpha}$ are shown in Fig. 14. At $M = 0.3$, $C_{m_q} + C_{m_\alpha}$ did not reveal any sting length effects (ℓ_{cr}/d undefined) but did show that the larger sting diameters produced lower levels of $C_{m_q} + C_{m_\alpha}$. The data at $M = 0.6$, 1.1, and 1.3 indicated no consistent diameter effects and also yielded an undefined value of ℓ_{cr}/d . Significant sting length effects were found, however, at $M = 0.95$. For this case, a decrease in ℓ_s/d resulted in a decrease in $C_{m_q} + C_{m_\alpha}$, and an ℓ_{cr}/d of 3 is apparent. A similar trend of decreased $C_{m_q} + C_{m_\alpha}$ with decreased ℓ_s/d at $M = 0.95$ was also observed on a flat-based 7-deg cone, as described in Refs. 3 and 4.

4.3.4 $C_{n_r} - C_{n\beta} \cos \alpha$ Measurement

Figure 15 depicts the variation of $C_{n_r} - C_{n\beta} \cos \alpha$ with ℓ_s/d for two sting diameters. Both sting length and diameter interference effects are obvious at Mach 0.95, 1.10, and 1.30. No consistent diameter effects are apparent at Mach number 0.6, and no conclusions can be made at $M = 0.3$ because of insufficient data. These trends show an obvious ℓ_{cr}/d of 4 at Mach number 0.95; at $M = 1.10$ and 1.30, the ℓ_{cr}/d is assumed to be 4. At $M = 0.6$, ℓ_{cr}/d is undefined for the range of ℓ_s/d investigated. These values of ℓ_{cr}/d apply only to a corresponding d_s/d of 0.4. A critical sting length is not made apparent by the data obtained with a d_s/d of 0.65. In summary, for the data in Fig. 15 at Mach numbers where interference effects were observed ($M = 0.95$, 1.10, and 1.30), sting length effects are characterized by an increase in yaw damping, whereas the sting diameter effect was generally characterized by a decrease in yaw damping.

4.3.5 p_b/p Measurement

The base-pressure measurements (nondimensionalized by the free-stream static pressure) are presented in Fig. 16 in three separate plots of p_b/p vs ℓ_s/d : one plot for each value of d_s/d (viz., 0.40, 0.65, and 0.73). Referring to the plot of $d_s/d = 0.4$ (Fig. 16a) makes the variation of p_b/p with ℓ_s/d immediately apparent, with clear definitions of ℓ_{cr}/d of 3 at $M = 1.3$ and 0.6, of 4 at $M = 1.1$, and of 5 at $M = 0.95$. Because the base-pressure ratio is very close to unity at $M = 0.3$, a definition of ℓ_{cr}/d is not attempted at this Mach number.

The data obtained with a d_s/d of 0.65 and 0.73 (Figs. 16b and 16c) are relatively similar, and essentially show a higher value of p_b/p at each Mach number and ℓ_s/d than do the data obtained with a d_s/d of 0.4 (Fig. 16a). It is not known why the data at an ℓ_s/d of 5.6 at each Mach number show a pronounced increase in p_b/p for $d_s/d = 0.65$ and 0.73 (Figs. 16b and 16c), but it is believed to be caused to some extent by the presence (or lack) of the conical Lexan flare (Fig. 4). At $\ell_s/d \leq 4$, this flare is mounted on the sting diameter tubes, whereas it is removed for an $\ell_s/d = 5.6$. Apparently, then, the flow expansion over the rearward edge of the Lexan flare produces a substantially different effect at the model base than does the steel flare over the motor housing (Fig. 3).

Nevertheless, Fig. 16 does indicate substantial sting diameter effects. In general, increasing the sting diameter increases p_b/p for all Mach numbers. Because of the suspected influence of the Lexan flare, it is not deemed appropriate to define ℓ_{cr}/d based on p_b/p for $d_s/d = 0.65$ and 0.73. Therefore, the evaluation of ℓ_{cr}/d as determined by p_b/p is based solely on data obtained for a d_s/d of 0.4, as previously discussed.

5.0 CONCLUDING REMARKS

Sting length and diameter interference effects as determined by the measurement of static and dynamic stability derivatives, static pitching moment, and base pressure were investigated at Mach numbers 0.30, 0.60, 0.95, 1.10, and 1.30. The nominal angle-of-attack range was from -4 to 14 deg. Data were obtained on the Standard Dynamics Model (SDM), at a nominal frequency of oscillation of 5.2 Hz. The primary unit Reynolds number at which the investigation was conducted was 2.5 million per foot, except for Mach number 0.95. At $M = 0.95$, the primary unit Reynolds number per ft was 1.0 million (pitch phase) and 1.5 million (yaw phase). Sting length was varied from 1 to 6 model diameters, for sting diameters of 0.40, 0.65, and 0.73 model diameters. Conclusions based on these results and a summary of critical sting length and diameter effects are as follows:

1. Sting Length Effects

- a. With exception of Mach number 0.95, the parameters C_m , $C_{m\alpha}$, $C_{n\beta} \cos \alpha$, and $C_{m\alpha} + C_{m\alpha}$ were essentially unaffected by sting length effects in the ℓ_s/d range from 2 to 6. Sting length interference effects were present at Mach number 0.95 and resulted in higher critical sting lengths than did the other Mach numbers.
- b. The yaw-damping derivative showed significant increases in damping due to sting length interference in the Mach range from 0.95 to 1.30. No effects were found at $M = 0.6$ for the ℓ_s/d range from 2 to 6.

- c. Sting length interference increased the model base pressure; depending on this measurement and on the Mach number, the critical sting length varied from 3 to 5 model diameters.
- d. Model oscillation amplitude did not alter the critical sting length determined by the measurement of pitch-damping derivatives.

2. Sting Diameter Effects

- a. The static stability parameters $C_{m\alpha}$ and $C_{n\beta} \cos \alpha$ were relatively independent of sting diameter effects.
- b. The pitch-damping derivatives showed a decrease in damping due to sting diameter effects at $M = 0.3$ for all values of ℓ/d . No significant sting diameter effects were observed in the pitch-damping derivatives at Mach numbers equal to or greater than 0.6.
- c. Sting diameter effects produced a decrease in yaw dynamic stability at $M = 1.3$ and at values of $\ell/d < 4$ at $M = 0.95$ and 1.10. No effects were observed at Mach number 0.6.
- d. Sting diameter effects on model base pressure were found at Mach numbers equal to and greater than 0.6 at all values of ℓ/d , and generally resulted in an increase in base pressure with an increase in sting diameter.

3. Overall Assessment of Interference on the SDM

The effects of sting length and diameter effects, as discussed above, are summarized in the chart on page 17.

Parameter	Mach Range	Sting Length Effects*	Sting Diameter Effects **
C_m	0.3 + 1.3	$l_{cr}/d \leq 2^+$	Not investigated.
$C_{m\alpha}$	0.3 + 1.3	$l_{cr}/d \leq 2^{++}$	None
$C_{n\beta} \cos \alpha$	0.6 + 1.3	$l_{cr}/d \leq 2$	None
$C_{m_q} + C_{m\alpha}$	0.3 + 1.3	$l_{cr}/d \leq 2^{++}$	Only at $M = 0.3$; damping decreased.
$C_{n_r} - C_{n\beta} \cos \alpha$	0.6 $>0.6 + 1.3$	$l_{cr}/d \leq 2$ $l_{cr}/d = 4$	No effect at $M = 0.6$. Decreased damping at $M = 1.3$ for all l_s/d and at $M = 0.95$ and 1.1 for $l_s/d < l_{cr}/d$.
Base Pressure	0.60 0.95 1.10 1.30	$l_{cr}/d \geq 4$ $l_{cr}/d = 5$ $l_{cr}/d = 4$ $l_{cr}/d = 3$	Significant at all Mach numbers and sting lengths investigated.

* a range of -4 to 14 deg

** Only $\alpha = 0$ Investigated

† Except $M = 0.95$, $l_{cr}/d = 5$

++ Except $M = 0.95$, $l_{cr}/d = 3$

REFERENCES

1. Uselton, Bob L. and Cyran, Fred B. "Critical Sting Length as Determined by the Measurement of Pitch-Damping Derivatives for Laminar, Transitional, and Turbulent Boundary Layers at Mach Number 3 for Reduced Frequencies of 0.0033 and 0.0056." AEDC-TR-77-66 (AD-A042747), July 1977.
2. Uselton, Bob L. and Cyran, Fred B. "Sting Interference Effects as Determined by Measurements of Dynamic Stability Derivatives, Surface Pressure, and Base Pressure for Mach Number 2 through 8." AEDC-TR-79-89, December 1979.
3. Cyran, Fred B., Uselton, Bob L., and Marquart, Ed. J. "Evaluation of Critical Sting Length on a 7-deg Cone as Determined by Measurements of Dynamic Stability Derivatives and Base Pressure for Mach Numbers 0.2 through 1.3." AEDC-TR-80-17, January 1981.
4. Cyran, Frederic B. "An Investigation of Sting Interference Effects on an Oscillating Cone in Transonic Flow." AEDC-TR-80-66 (to be published).
5. Cyran, F. B. and Chaney, M. J. "Sting Interference Effects on the SDM Aircraft as Determined by Measurements of Dynamic Stability Derivatives and Base Pressure for Mach Numbers 0.3 through 1.3." AEDC-TR-80-P70, October 1980.
6. *Test Facilities Handbook* (Eleventh Edition). "Propulsion Wind Tunnel Facility, Vol. 4." Arnold Engineering Development Center, June 1979.
7. Burt, G. E. "A Description of a Pitch/Yaw Dynamic Stability, Forced-Oscillation Test Mechanism for Testing Lifting Configurations." AEDC-TR-73-60 (AD762286), June 1973.
8. Schueler, C. J., Ward, L. K., and Hodapp, A. E. "Techniques for Measurement of Dynamic Stability Derivatives in Ground Test Facilities." AGARDograph 121 (AD669227), October 1967.
9. Abernethy, R. B. et al. (Pratt and Whitney) and Thompson, J. W. (ARO, Inc). "Handbook Uncertainty in Gas Turbine Measurements." AEDC-TR-73-5 (AD755356), February 1973.
10. "USAF Stability and Control DATCOM." Flight Control Division, Air Force Flight Dynamics Laboratory, Wright-Patterson Air Force Base, Ohio. Revised January 1975.

11. Uselton, James C., Uselton, Bob L., and Helmlinger, K. R. "An Examination of the Small-Amplitude Dynamic Stability Test Technique." AEDC-TR-74-131 (AD-A008477), April 1975.
12. Mark, Andrew. "Free-Flight Base Pressure Measurements on 8-deg Cones." ARBRL-TR-02179, July 1979.

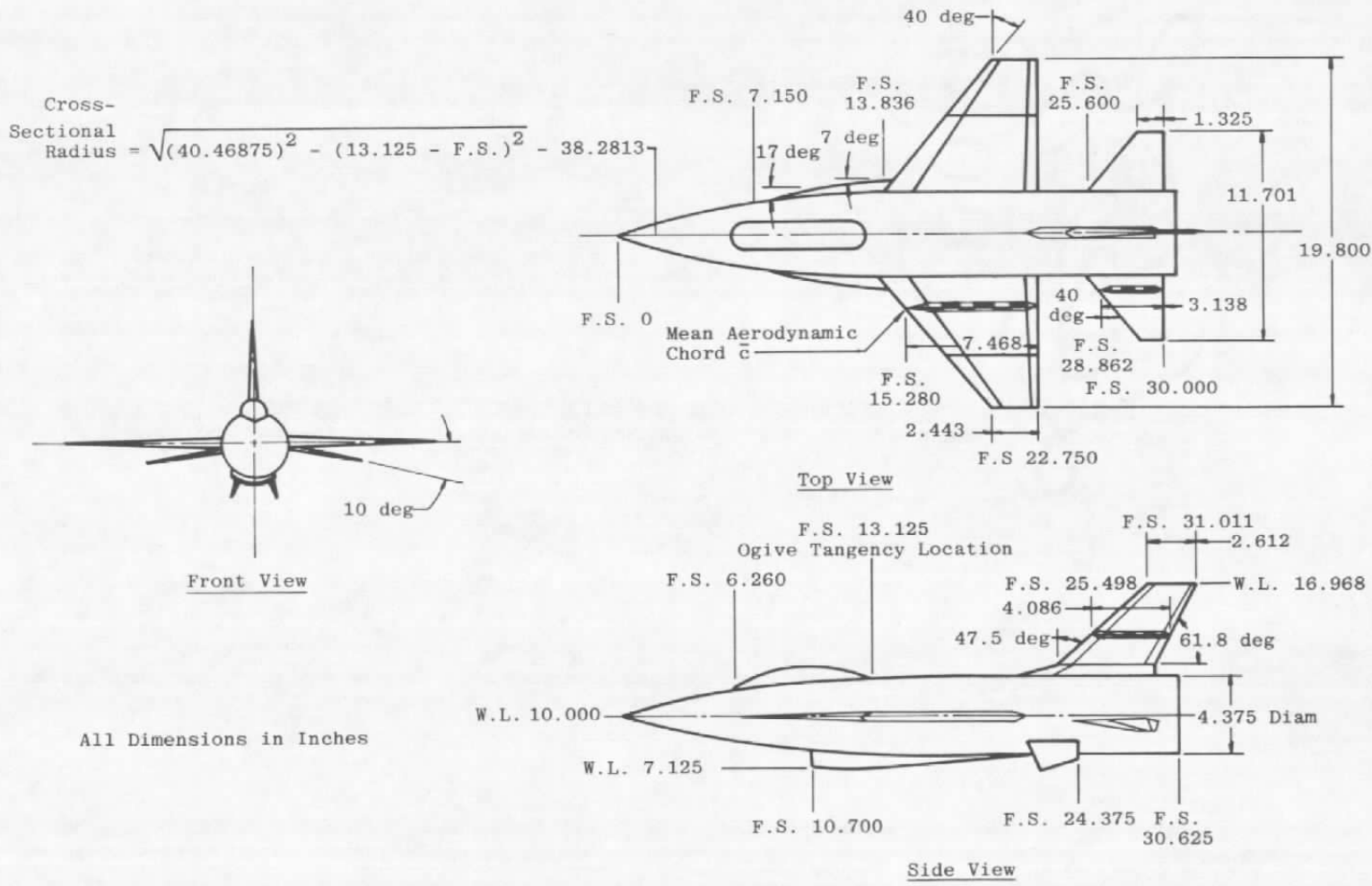


Figure 1. Standard dynamics model (SDM) details.

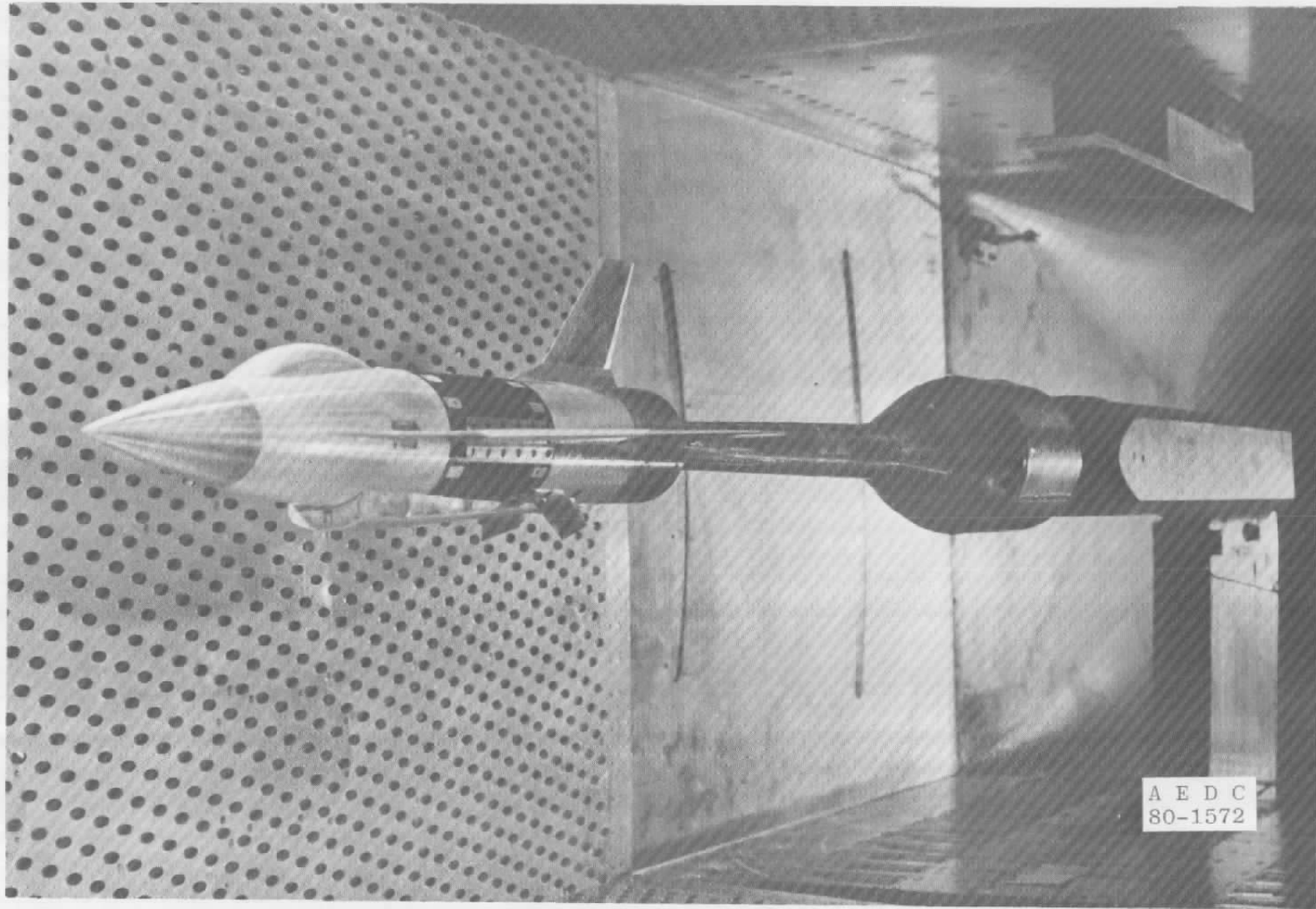
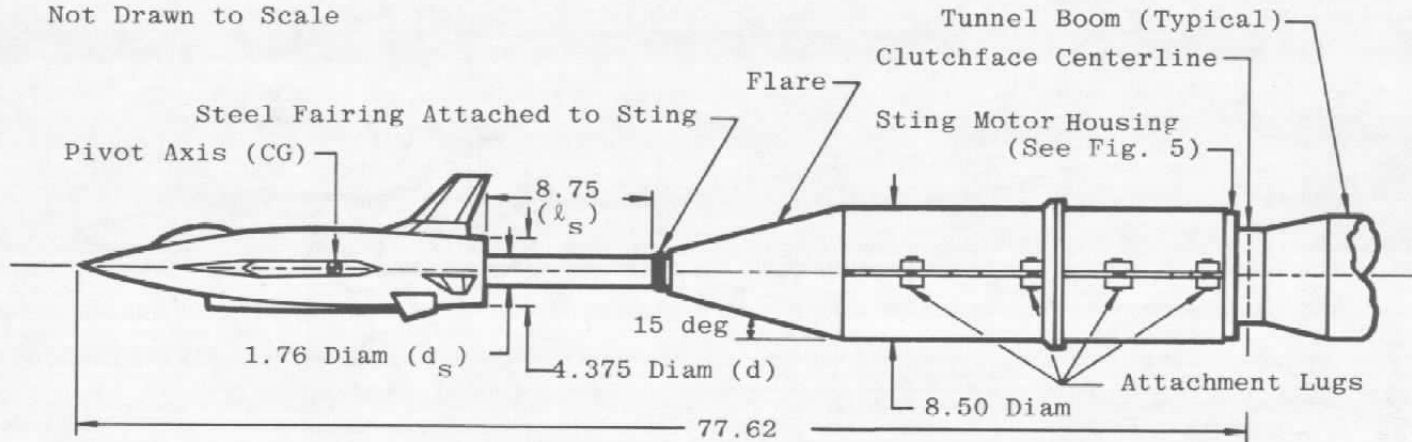


Figure 2. Photograph of model installation in Aerodynamic Wind Tunnel (4T).

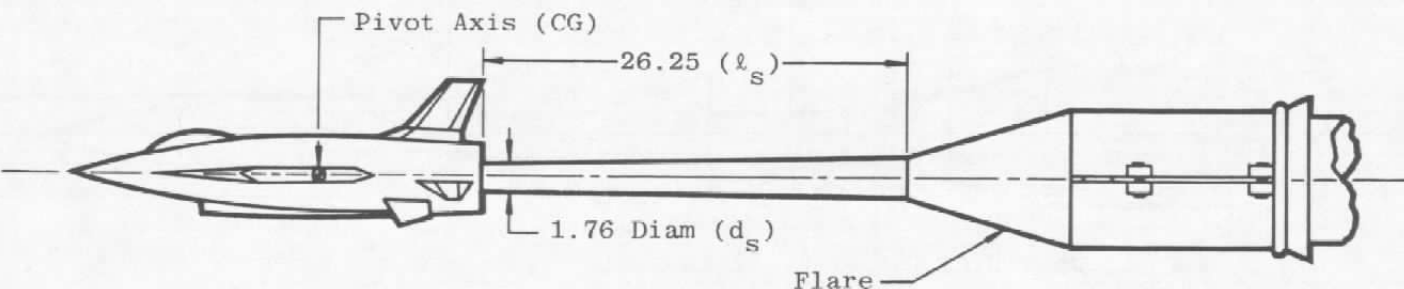
All Dimensions in Inches

Model Configuration Shown +B1C1W1V1T00S1F1II1

Not Drawn to Scale



$$a. \frac{l_s}{d} = 2.0, \frac{d_s}{d} = 0.40$$



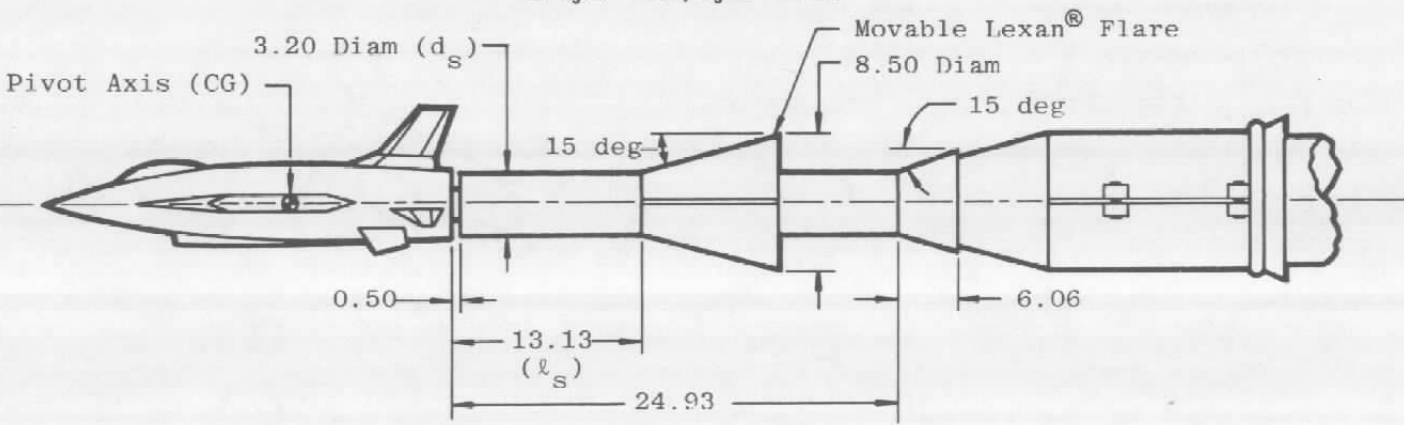
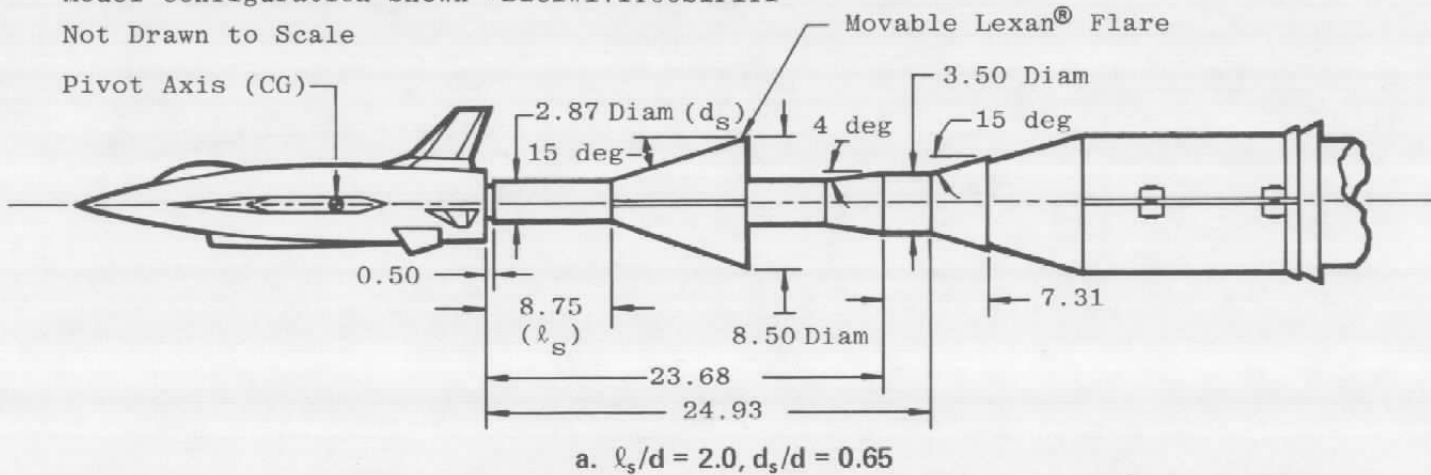
$$b. \frac{l_s}{d} = 6.0, \frac{d_s}{d} = 0.40$$

Figure 3. Details of model support configurations, $d_s/d = 0.40$.

All Dimensions in Inches

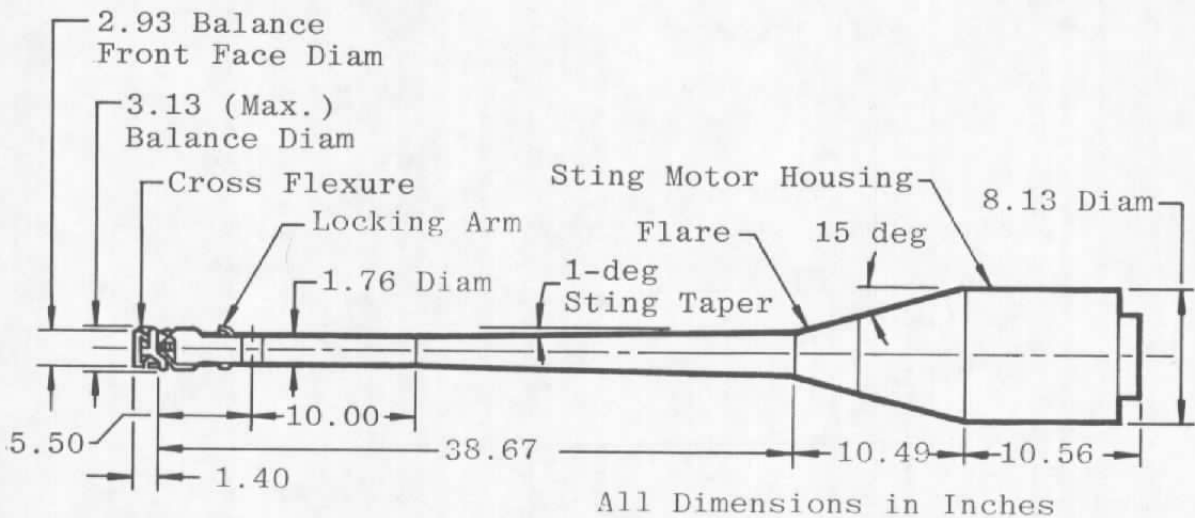
Model Configuration Shown +B1C1W1V1T00S1F1I1

Not Drawn to Scale

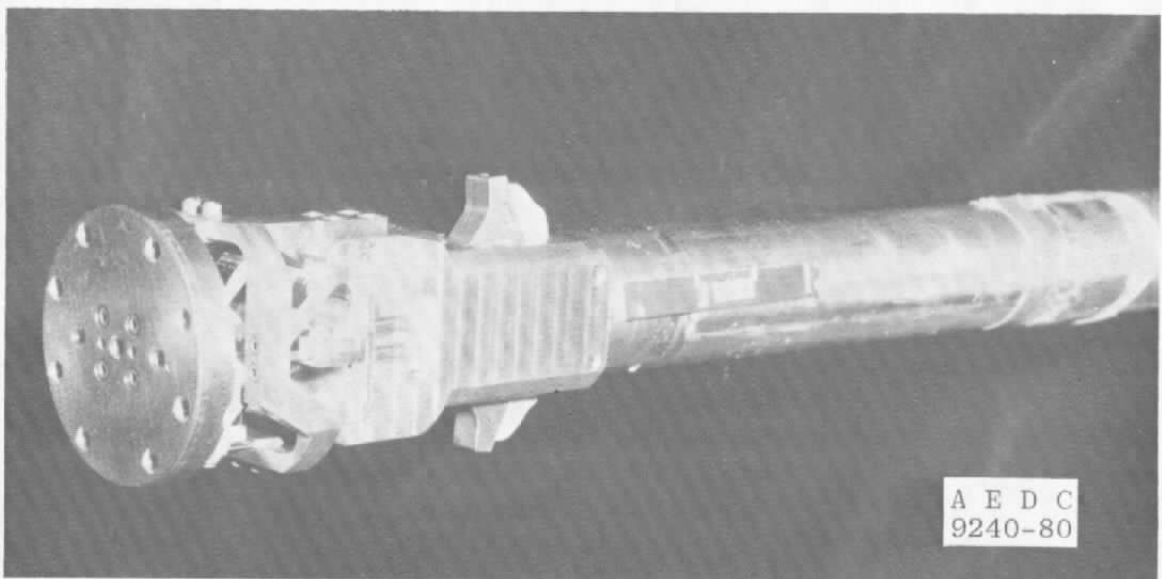


b. $l_s/d = 3.0$, $d_s/d = 0.73$

Figure 4. Details of model support configurations, $d_s/d = 0.65$ and 0.73 .



a. Details of test mechanism

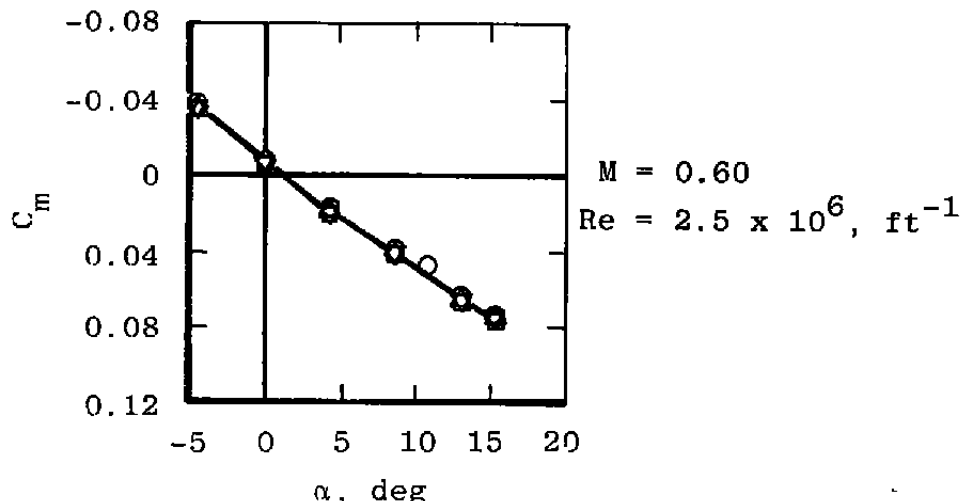


b. Photograph of cross flexure pivot

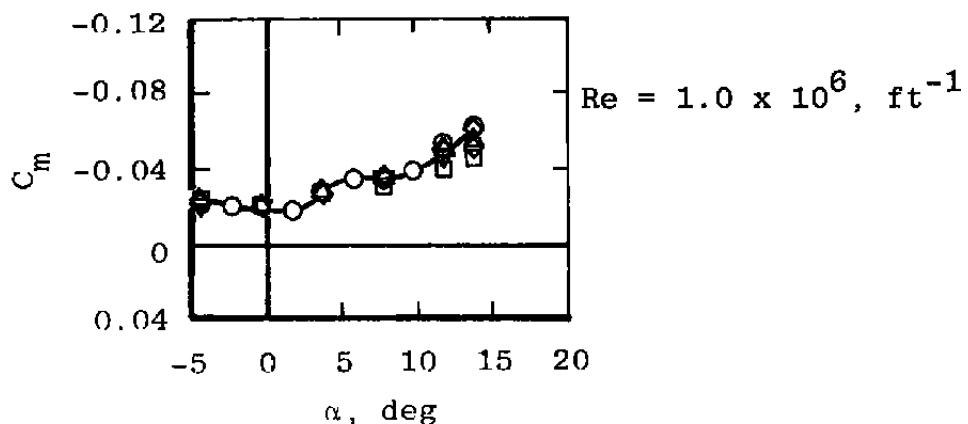
Figure 5. Details and photograph of VKF 1.C forced-oscillation test mechanism.

Sym	$\frac{\ell_s}{d}$	$\frac{d_s}{d}$
○	6.0	0.40
◊	5.0	
△	4.0	
▽	3.0	
□	2.0	

Configuration +B1C1W1V1T00S1F1I1

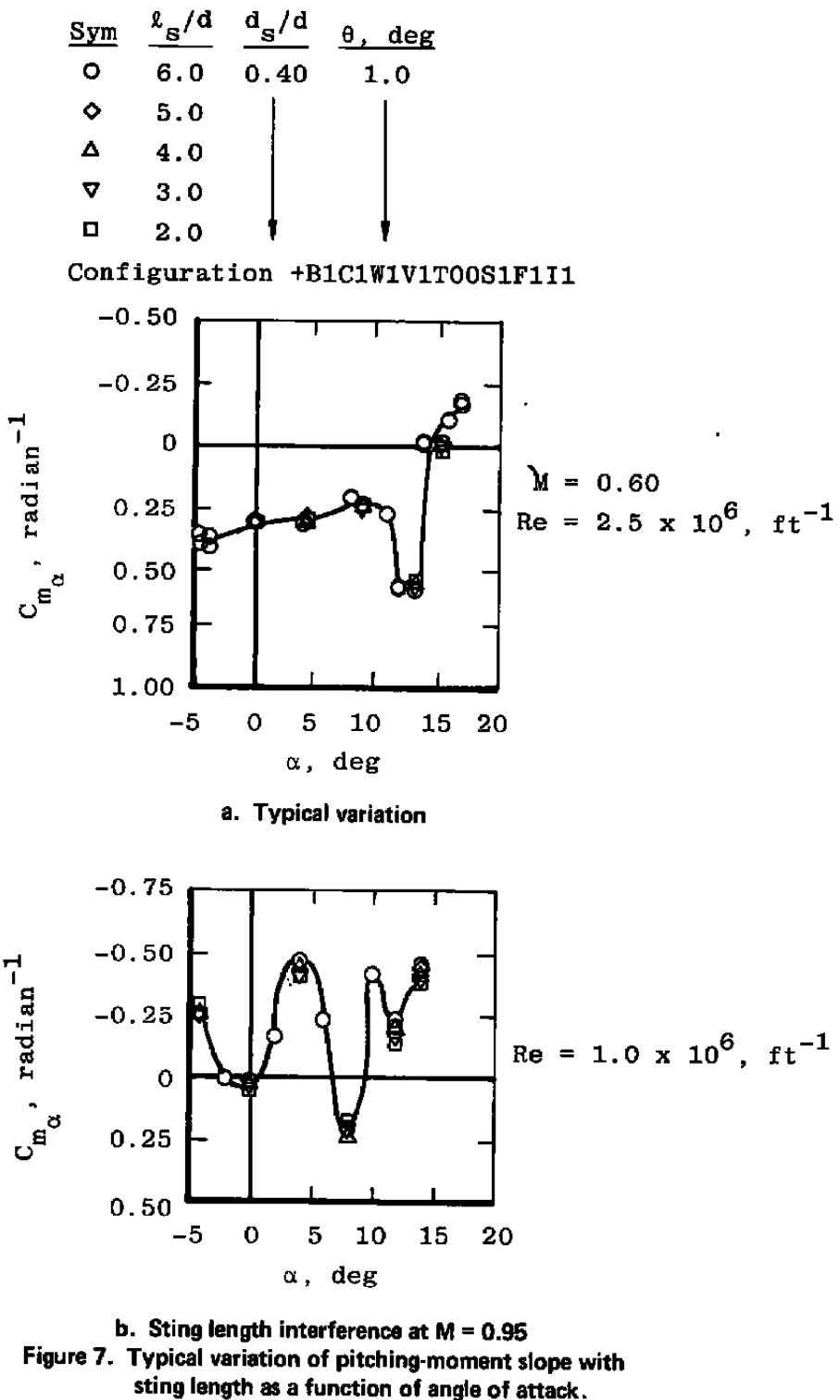


a. Typical variation



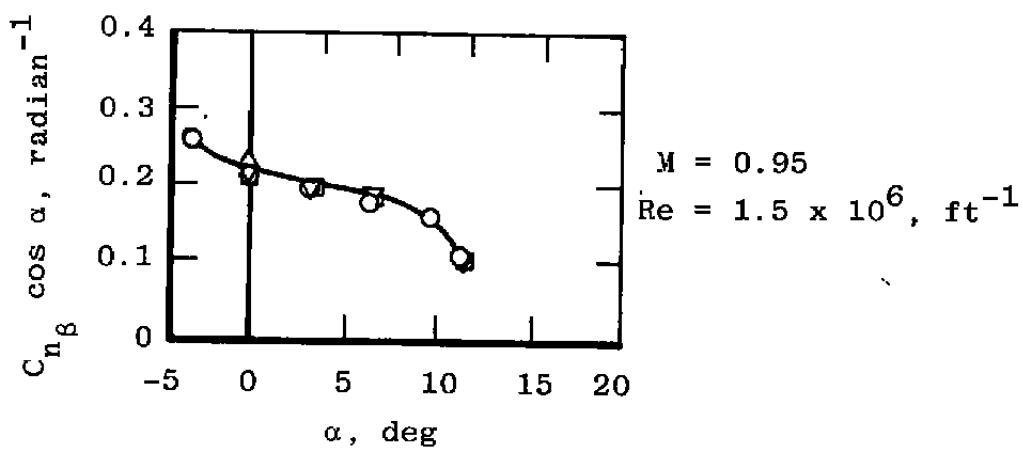
b. Sting length interference at $M = 0.95$

Figure 6. Variation of pitching moment with sting length as a function of angle of attack.

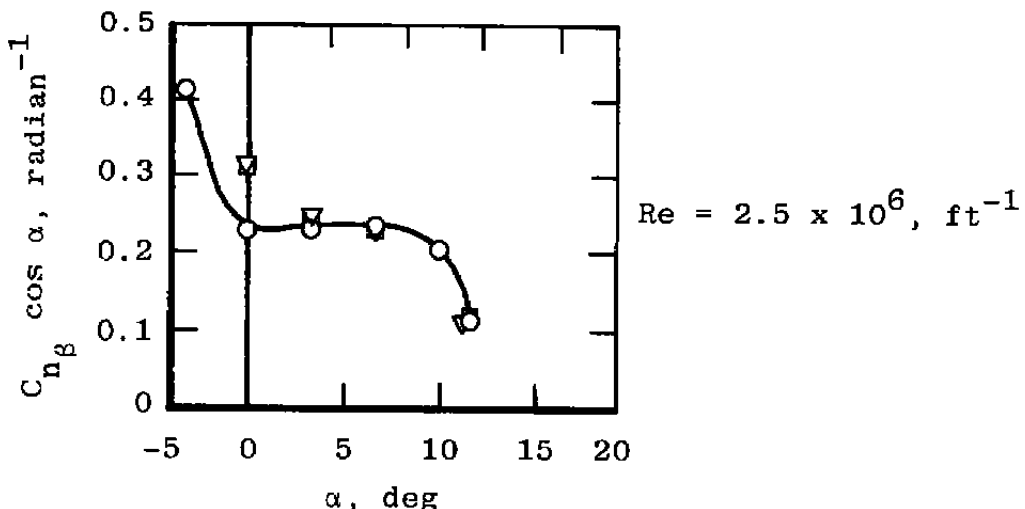


Sym	$\frac{l_s}{d}$	$\frac{d_s}{d}$	θ , deg
○	6.0	0.40	1.0
◊	5.0		
△	4.0		
▽	3.0		
□	2.0		

Configuration -B1C1W1V1T05S1F1I1



a. Typical variation

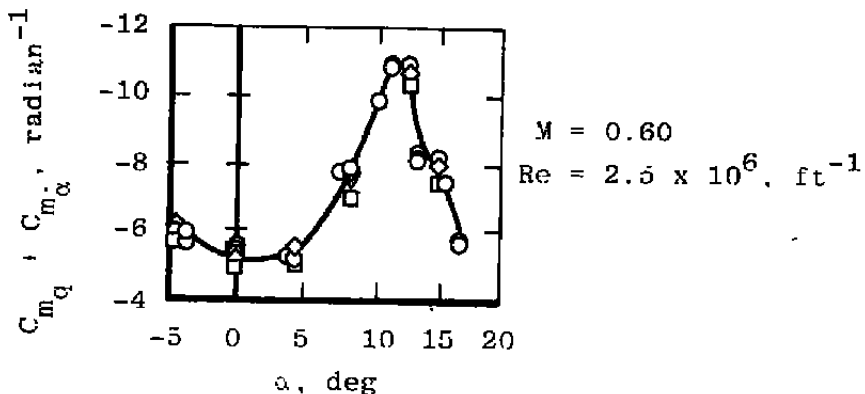


b. Sting length interference at $M = 1.1$

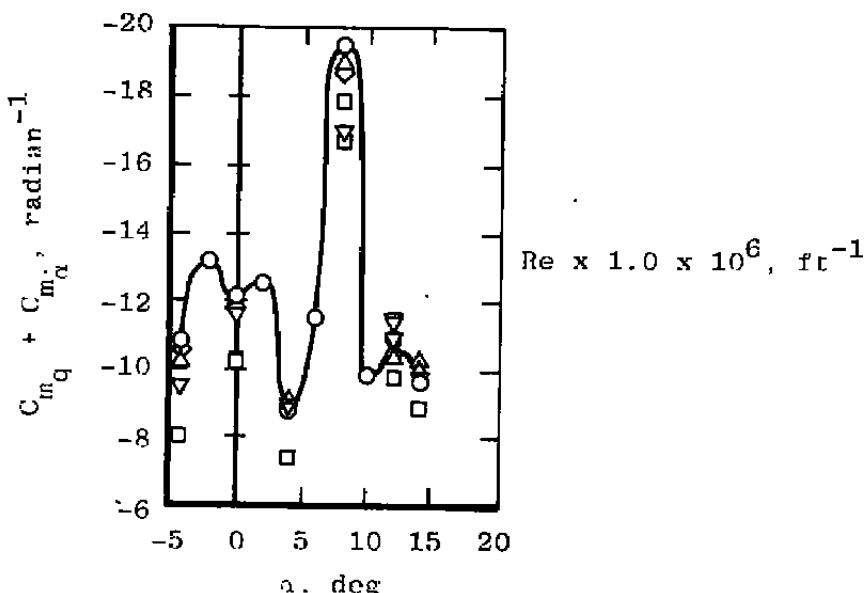
Figure 8. Variation of yawing-moment slope with sting length as a function of angle of attack.

Sym	$\frac{\ell_s}{d}$	$\frac{d_s}{d}$	θ , deg
○	6.0	0.40	1.0
◊	5.0		
△	4.0		
▽	3.0		
□	2.0		

Configuration +B1C1W1V1T00S1F1I1



a. Typical variation



b. Sting length interference at $M = 0.95$

Figure 9. Variation of pitch-damping derivatives with sting length as a function of angle of attack.

Sym	$\frac{l_s}{d}$	$\frac{d_s}{d}$	$\theta, \text{ deg}$
○	6.0	0.40	1.0
▽	3.0		
□	2.0		

Configuration -B1C1W1V1T05S1F1I1

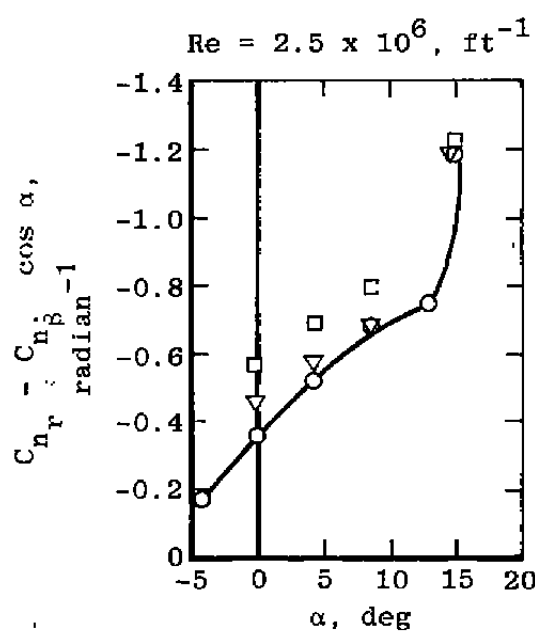
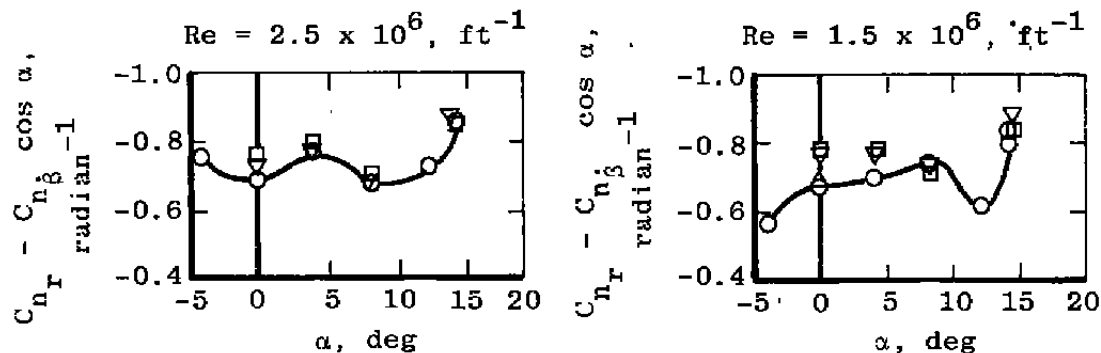
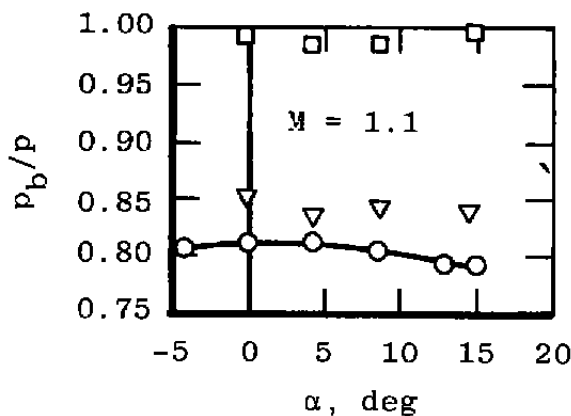


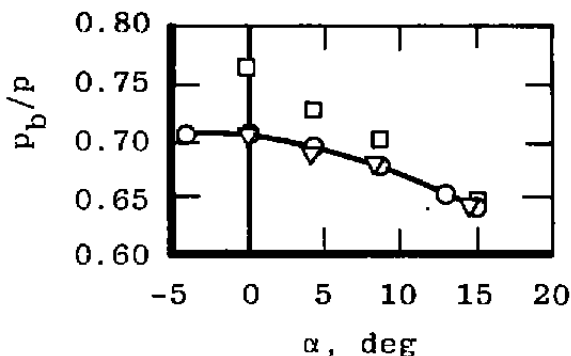
Figure 10. Variation of yaw-damping derivatives with sting length as a function of angle of attack.

Sym	$\frac{l_s}{d}$	$\frac{d_s}{d}$	$\frac{Re \times 10^6}{ft^{-1}}$
○	6.0	0.40	2.5
▽	3.0		
□	2.0		

Configuration -B1C1W1V1T05S1F1I1

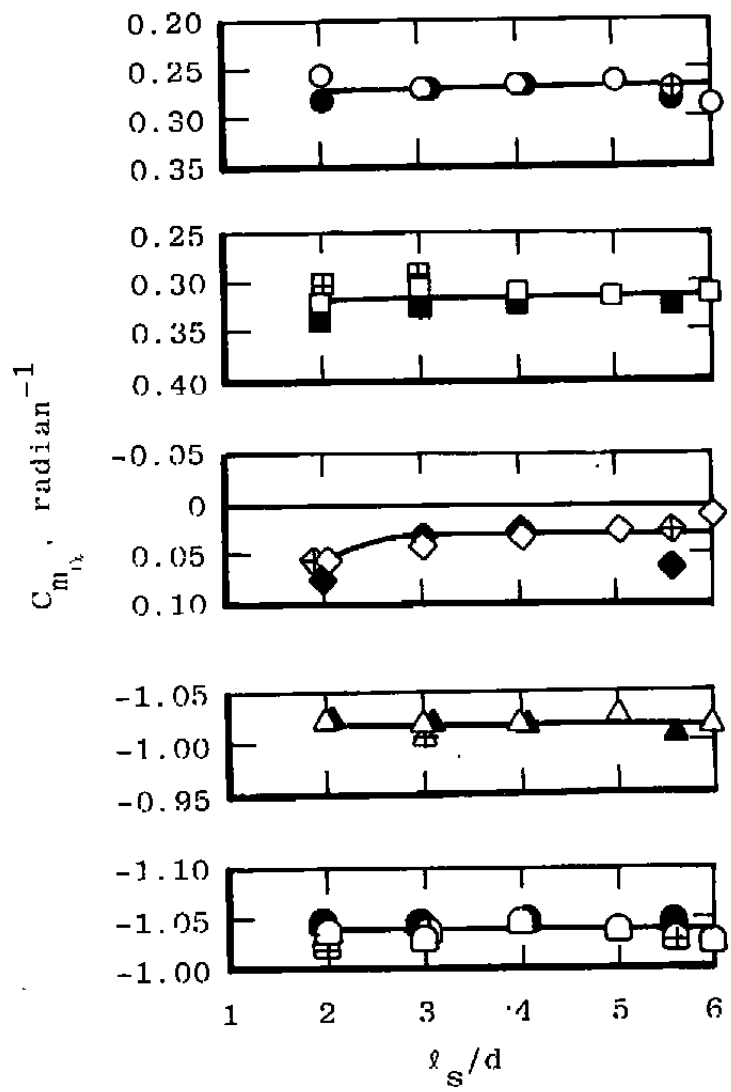


a. Typical variation



b. Sting length interference at $M = 1.3$

Figure 11. Variation of base-pressure ratio with sting length as a function of angle of attack.

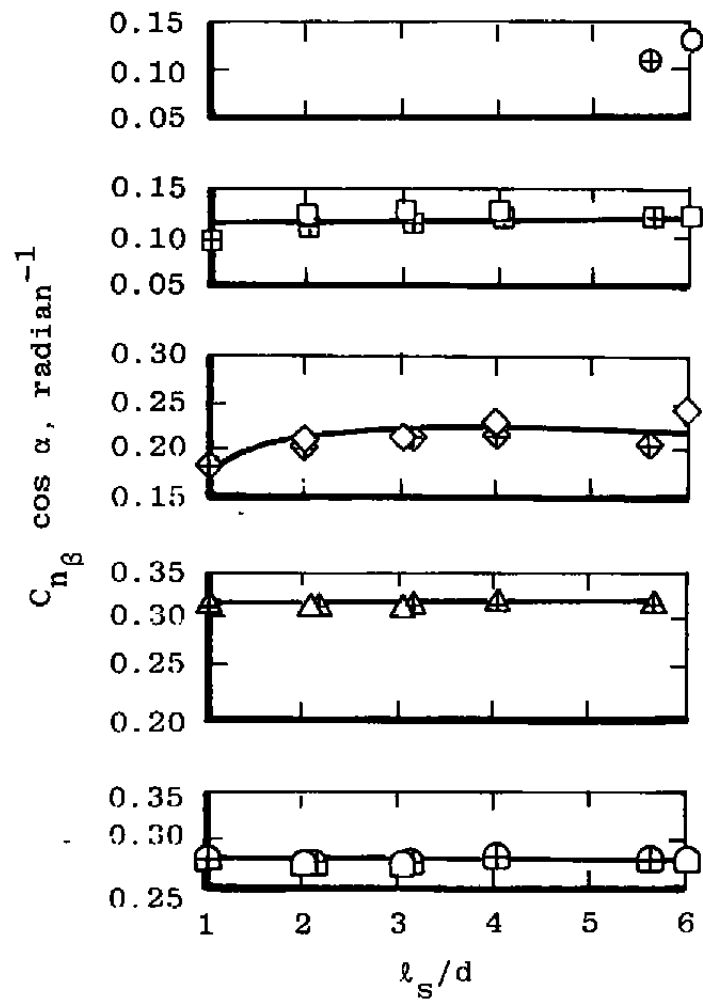


<u>Sym</u>	<u>M</u>	<u>$R_e \times 10^{-6}$, ft⁻¹</u>	<u>θ, deg</u>	<u>α, deg</u>
○	0.30	2.5	1.0	0
□	0.60	2.5		
◊	0.95	1.0		
△	1.10	2.5		
□	1.30	2.5		

Configuration +B1C1W1V1T00S1F1I1

<u>Sym</u>	<u>d_s/d</u>
Open	0.40
Crossed	0.65
Solid	0.73

Figure 12. Variation of pitching-moment slope with sting length for various sting diameters.

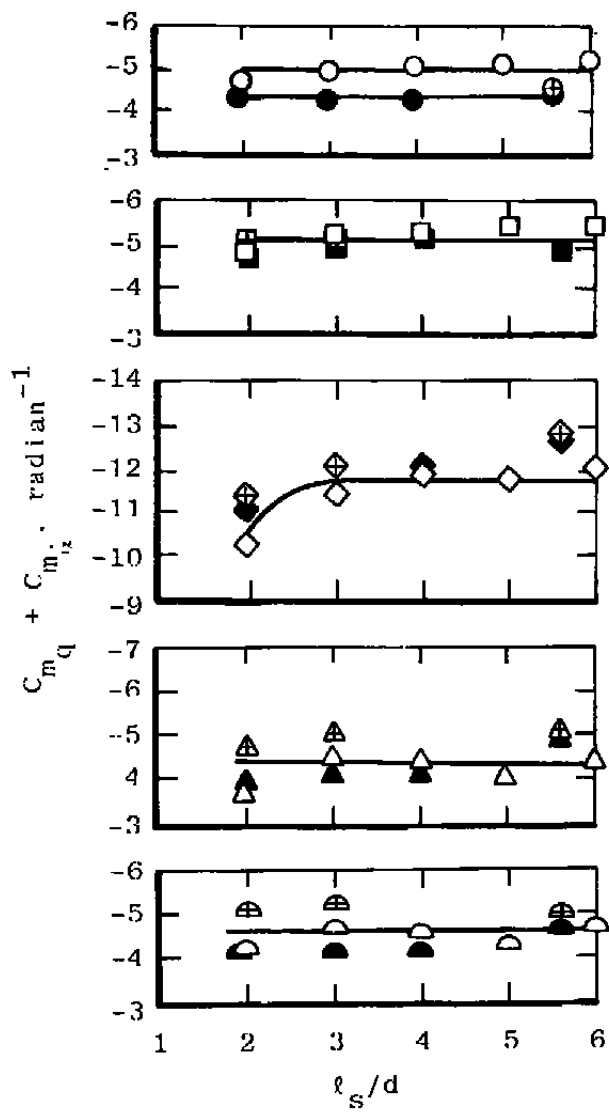


Symbol	M	$Re \times 10^{-6}, \text{ ft}^{-1}$	$\theta, \text{ deg}$	$\alpha, \text{ deg}$
○	0.30	2.5	1.0	0
□	0.60	2.5		
◇ (⊕)	0.95	1.0(1.5)		
△	1.10	2.5		
□	1.30	2.5		

Configuration ~B1C1W1V1T05S1F1I1

Symbol	d_s / d
Open	0.40
Crossed	0.65

Figure 13. Variation of yawing-moment slope with sting length for various sting diameters.

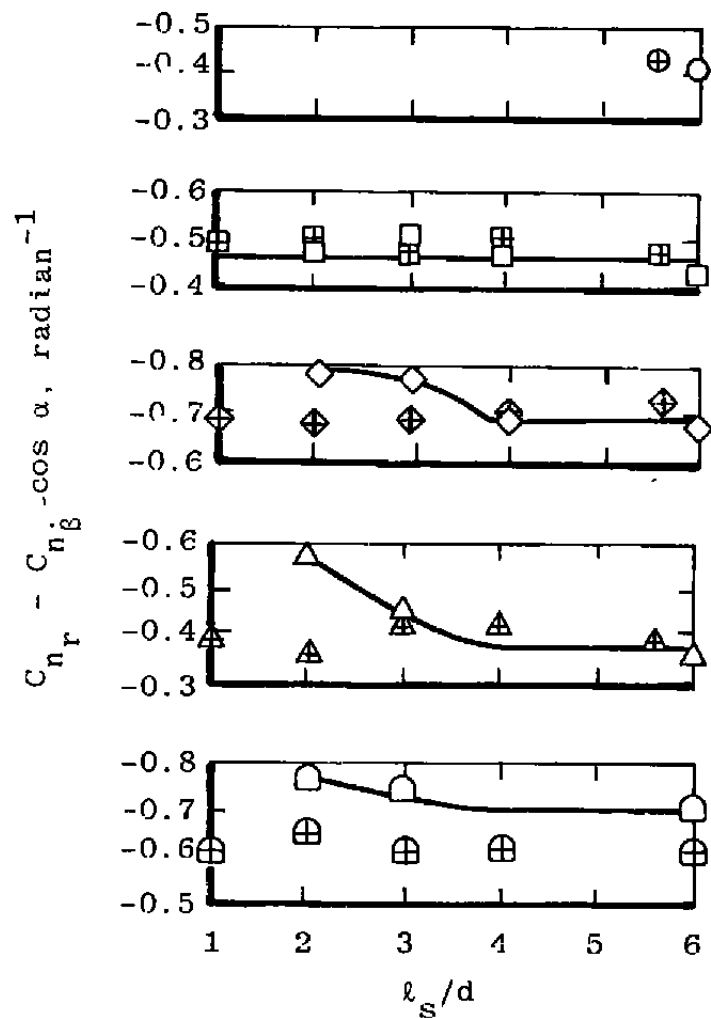


<u>Sym</u>	<u>M</u>	<u>Re x 10⁻⁶</u> , ft ⁻¹	<u>θ</u> , deg	<u>α</u> , deg
○	0.30	2.5	1.0	0
□	0.60	2.5		
◊	0.95	1.0		
△	1.10	2.5		
□	1.30	2.5		

Configuration +B1C1W1V1T00S1F1I1

<u>Sym</u>	<u>d_s/d</u>
Open	0.40
Crossed	0.65
Solid	0.73

Figure 14. Variation of pitch-damping derivatives with sting length for various sting diameters.



Symbol	M	$Re \times 10^{-6}$, ft $^{-1}$	θ , deg	α , deg
○	0.30	2.5	1.0	0
□	0.60	2.5		
◇(⊕)	0.95	1.0(1.5)		
△	1.10	2.5		
□	1.30	2.5		

Configuration -B1C1W1V1T05S1F1I1

Symbol	d_s/d
Open	0.40
Crossed	0.65

Figure 15. Variation of yaw-damping derivatives with sting length for various sting diameters.

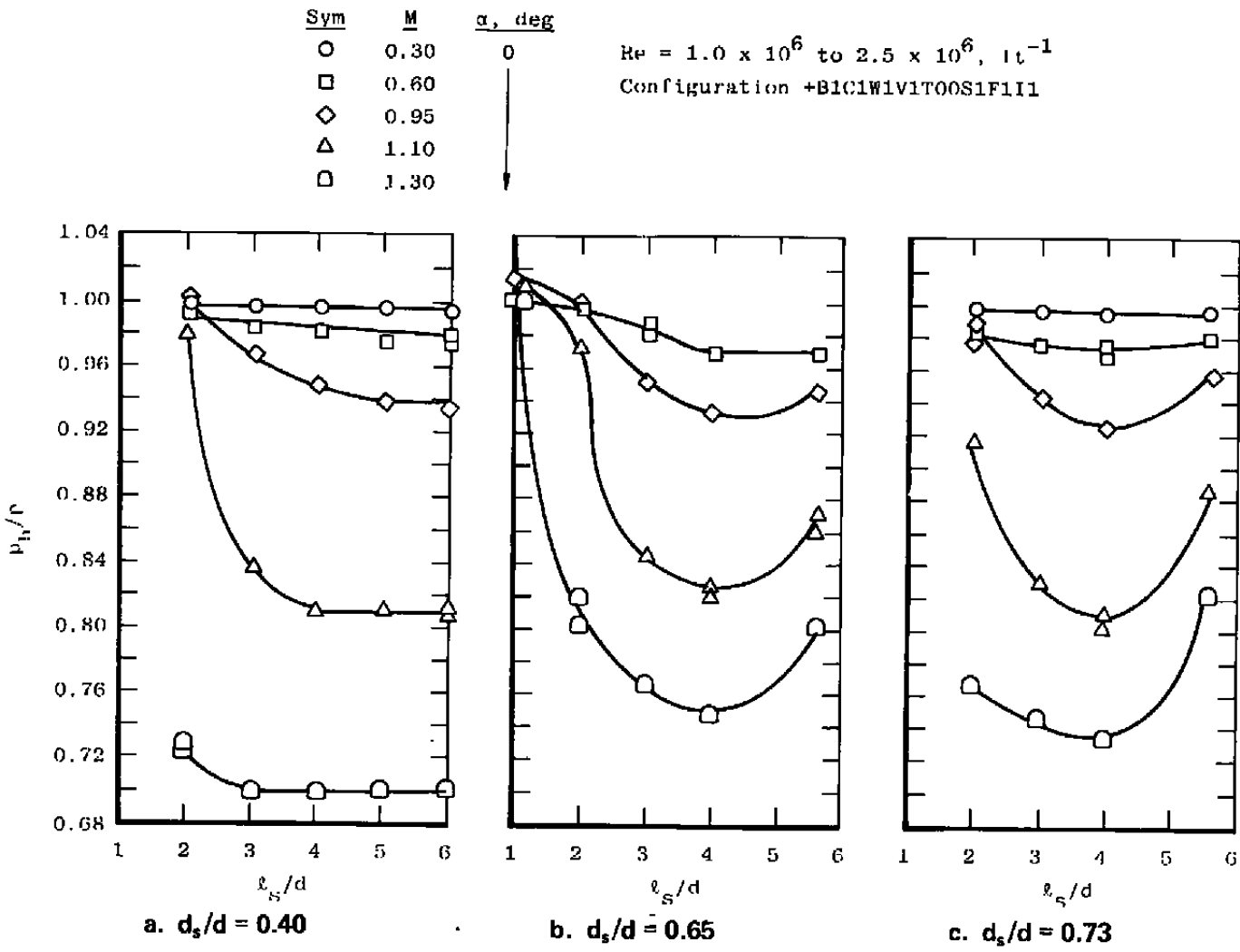


Figure 16. Variation of base-pressure ratio with sting length for various sting diameters.

Table 1. Standard Dynamics Model (SDM) Dimensions

WING	
Area (A)	0.90702 ft ²
Span (b)	1.6500 ft
Mean Aerodynamic Chord (c)	0.62233 ft
Aspect Ratio	3.0
L.E. Sweep	40 deg
Dihedral	0
Incidence	0
Airfoil	Double wedge; 4.5 percent thickness at root.
L.E. Angle	15 deg (Half Angle)
T.E. Angle	15 deg (Half Angle)
HORIZONTAL TAIL	
Area	0.30707 ft ²
Aspect Ratio	3.0
Taper Ratio	0.213
L.E. Sweep	40 deg
Dihedral	-10 deg
Airfoil	Double wedge; 6.4 percent thickness at root.
L.E. Angle	14 deg (Half Angle)
T.E. Angle	15 deg (Half Angle)
VERTICAL TAIL	
Area	0.30846 ft ²
Aspect Ratio	1.093
Taper Ratio	0.362
L.E. Sweep	
Tip	47.5 deg
Root	15.0 deg
Airfoil	Double wedge; 5.6 percent thickness at root.
L.E. Angle	15 deg (Half Angle)
T.E. Angle	15 deg (Half Angle)
VENTRAL FIN (Each)	
Area	0.0263 ft ²
Span	0.150 ft
Aspect Ratio	0.86
Taper Ratio	0.70
L.E. Sweep	26.5 deg
Dihedral (cant)	25.2 deg (Outboard)
Airfoil	Modified wedge; 3.8 percent thick at root.
At Root	Constant 0.003 radian
At Tip	
FUSELAGE	
Length	2.55208 ft
Diameter (d)	0.36458 ft
Center of Gravity (CG)	1.49125 ft from Nose at 35-percent c 1.36667 from Nose at 15-percent c

Table 2. Standard Dynamics Model (SDM) Configuration Codes

<u>Configuration</u>	<u>Description (Refer to Fig. 1)</u>
+B1C1W1V1T00S1F1I1	BODY + CANOPY + WINGS + VERTICAL TAIL + HORIZONTAL STABILIZERS + STRAKES + VENTRAL FINS + INLET; Horizontal Stabilizer Deflection Angle = 0; CG Located at 35 percent of \bar{c} (F.S. = 17.895)
-B1C1W1V1T05S1F1I1	Same as +B1C1W1T00S1F1I1, Except Horizontal Stabilizer Deflection Angle = -5 deg (Positive Trailing Edge Down)
-B2C1W1V1T05S1F1I1	Same as -B1C1W1T05S1F1I1, Except CG Located at 15 percent of \bar{c} (F.S. = 16,400)

Table 3. Test Conditions

M	<u>p_t, psfa</u>	<u>T_t, °R</u>	<u>q, psf</u>	<u>p, psf</u>	<u>v, ft/sec</u>	<u>$Re \times 10^{-6}$, ft$^{-1}$</u>	<u>$Re_c \times 10^6$</u>
0.30	575	562	34	540	346	0.5	0.3
0.30	1,112	549	66	1,045	342	1.0	0.6
0.30	2,017	571	118	1,867	349	1.7	1.0
0.30	2,966	583	180	2,812	354	2.5	1.6
0.30	3,670	592	217	3,441	355	3.0	1.9
0.60	641	559	127	503	671	1.0	0.6
0.60	1,608	563	318	1,261	674	2.5	1.6
0.60	3,374	583	664	2,642	685	5.0	3.1
0.80	723	544	212	474	861	1.4	0.9
0.95	486	551	172	273	1,004	1.0	0.6
0.95	754	562	267	420	1,019	1.5	0.9
0.95	823	546	291	460	1,002	1.7	1.0
0.95	1,207	549	427	676	1,004	2.5	1.6
1.05	849	548	326	424	1,089	1.8	1.1
1.05	1,201	558	463	596	1,104	2.5	1.6
1.10	1,196	557	474	561	1,141	2.5	1.6
1.20	983	550	409	409	1,215	2.1	1.3
1.30	1,200	554	512	434	1,296	2.5	1.6

Table 4. Test Summary
a. Pitch-Damping

Run	d_s/d	l_s/d	M	$Re \times 10^{-6}$, ft $^{-1}$	p_t , psfa	θ , deg	$\omega_d/2V$, radian	α , deg
Configuration +B1C1W1V1T00S1F1I1								
31	0.40	6.0	0.60	2.5	1,608	1.0	0.015	0, -4
31	0.40	6.0	0.60	2.5	1,632	1.0	0.015	-4 → 17
33	0.40	6.0	0.60	2.5	1,629	2.0	0.015	0
34	0.40	6.0	0.60	5.0	3,367	1.0	0.014	0, -4
42	0.40	6.0	0.60	2.5	1,615	1.0	0.015	-4 → 15
43	0.40	6.0	0.60	2.5	1,615	2.0	0.015	0
44	0.40	6.0	0.60	5.0	3,328	1.0	0.014	-6 → 7
45	0.40	6.0	0.60	1.0	640	1.0	0.015	-4 → 14
50	0.40	6.0	0.95	2.5	1,207	1.0	0.010	0, -4
54	0.40	6.0	0.95	1.0	487	1.0	0.010	-4 → 14
55	0.40	6.0	0.95	1.0	500	2.0	0.010	0
56	0.40	6.0	0.30	2.5	2,989	1.0	0.030	0
61	0.40	6.0	0.30	2.5	2,930	1.0	0.030	-4 → 15
62	0.40	6.0	0.30	2.5	2,962	2.0	0.030	0
63	0.40	6.0	0.30	2.5	2,971	1.0	0.030	0
64	0.40	6.0	0.30	3.0	3,663	1.0	0.030	0
65	0.40	6.0	0.30	1.7	1,989	1.0	0.032	0
66	0.40	6.0	0.30	0.5	575	1.0	0.031	0
67	0.40	6.0	1.05	2.5	1,200	1.0	0.010	0
68	0.40	6.0	1.10	2.5	1,200	1.0	0.010	-4 → 2
70	0.40	6.0	1.10	2.5	1,202	2.0	0.010	0
72	0.40	6.0	1.30	2.5	1,200	1.0	0.009	-2 → 3
73	0.40	6.0	1.30	2.5	1,200	2.0	0.009	0
83	0.40	5.0	0.30	2.5	2,874	1.0	0.030	-4 → 15
84	0.40	5.0	0.60	2.5	1,632	1.0	0.015	-5 → 15
85	0.40	5.0	0.95	1.0	486	1.0	0.011	-4 → 14
86	0.40	5.0	0.95	1.0	486	2.0	0.011	0
87	0.40	5.0	1.10	2.5	1,180	1.0	0.010	0, 1, 3
88	0.40	5.0	1.10	2.5	1,180	2.0	0.010	0
89	0.40	5.0	1.30	2.5	1,185	1.0	0.009	-2 → 3

Table 4. Continued
a. Continued

Run	d_s/d	l_s/d	M	$Re \times 10^{-6}$ ft $^{-1}$	P_t , psfa	θ , deg	$\omega d/2V$, radian	α , deg
Configuration +B1C1W1V1T00S1F1I1								
90	0.40	5.0	1.30	2.5	1,185	2.0	0.009	0
93	0.40	2.0	0.30	2.5	2,846	1.0	0.031	-4 → 15
94	0.40	2.0	0.30	2.5	2,846	2.0	0.031	0
95	0.40	2.0	0.60	2.5	1,609	1.0	0.015	-5 → 15
96	0.40	2.0	0.60	2.5	1,609	2.0	0.015	0
101	0.40	2.0	0.95	1.0	495	2.0	0.011	0
102	0.40	2.0	0.95	1.0	495	1.0	0.011	-4 → 14
103	0.40	2.0	1.10	2.5	1,188	1.0	0.010	-2 → 3
104	0.40	2.0	1.30	2.5	1,178	1.0	0.009	-2 → 3
105	0.40	2.0	1.30	2.5	1,182	2.0	0.009	0
108	0.40	3.0	0.30	2.5	2,888	1.0	0.030	0
109	0.40	3.0	0.30	2.5	2,915	1.0	0.030	-4 → 15
110	0.40	3.0	0.30	2.5	2,928	2.0	0.030	0
112	0.40	3.0	0.60	2.5	1,623	2.0	0.015	0
113	0.40	3.0	0.60	2.5	1,624	1.0	0.015	0
114	0.40	3.0	0.95	1.0	500	1.0	0.011	-4 → 14
115	0.40	3.0	0.95	1.0	500	2.0	0.010	0
116	0.40	3.0	1.10	2.5	1,187	1.0	0.010	-2 → 3
117	0.40	3.0	1.10	2.5	1,194	2.0	0.010	0
118	0.40	3.0	1.30	2.5	1,185	1.0	0.009	-2 → 3
119	0.40	3.0	1.30	2.5	1,187	1.0	0.009	0
120	0.40	3.0	0.60	2.5	1,606	2.0	0.015	0, 9
127	0.40	4.0	0.30	2.5	2,914	1.0	0.030	0, 4, 8
128	0.40	4.0	0.30	2.5	2,935	2.0	0.030	0
129	0.40	4.0	0.60	2.5	1,640	1.0	0.015	0
130	0.40	4.0	0.95	1.0	500	1.0	0.010	-4 → 14
131	0.40	4.0	0.95	1.0	500	2.0	0.010	0
132	0.40	4.0	1.10	2.5	1,191	2.0	0.010	0
133	0.40	4.0	1.10	2.5	1,194	1.0	0.010	0
134	0.40	4.0	1.30	2.5	1,196	1.0	0.009	-2 → 3
135	0.40	4.0	1.30	2.5	1,192	2.0	0.009	0

Table 4. Continued
a. Continued

Run	d_s/d	z_s/d	M	$Re \times 10^{-6}$, ft $^{-1}$	p_t , psfa	θ , deg	$wd/2V$, radian	α , deg
Configuration +B1C1W1V1T00S1F1I1								
143	0.73	5.6	0.30	2.5	2,928	1.0	0.030	-4—15
144	0.73	5.6	0.60	2.5	1,622	1.0	0.015	-5—15
145	0.73	5.6	0.95	1.0	492	1.0	0.011	-4—12
146	0.73	5.6	1.10	2.5	1,196	1.0	0.010	0
147	0.73	5.6	1.10	2.5	1,195	1.0	0.010	-2,1,3
148	0.73	5.6	1.30	2.5	1,194	1.0	0.009	0, -2
149	0.73	5.6	1.30	2.5	1,184	1.0	0.010	-3, 3
152	0.73	4.0	0.30	2.5	2,900	1.0	0.030	-4—15
153	0.73	4.0	0.60	2.5	1,589	1.0	0.015	-5—15
157	0.73	4.0	0.30	2.5	2,889	1.0	0.030	0,-4,4
158	0.73	4.0	0.60	2.5	1,625	1.0	0.015	0,-4,4
159	0.73	4.0	0.95	1.0	497	1.0	0.010	-4—14
161	0.73	4.0	1.10	2.5	1,191	1.0	0.010	-2—3
162	0.73	4.0	1.30	2.5	1,190	1.0	0.009	-2—3
165	0.73	3.0	0.30	2.5	2,879	1.0	0.030	-4—15
166	0.73	3.0	0.60	2.5	1,593	1.0	0.015	-5—13
167	0.73	3.0	0.95	1.0	492	1.0	0.011	-4—14
168	0.73	3.0	1.10	2.5	1,191	1.0	0.010	-2—3
169	0.73	3.0	1.30	2.5	1,185	1.0	0.009	-2—3
172	0.73	2.0	0.30	2.5	2,883	1.0	0.030	-4—15
173	0.73	2.0	0.60	2.5	1,594	1.0	0.015	-5—15
174	0.73	2.0	0.95	1.0	486	1.0	0.010	-4—14
175	0.73	2.0	1.10	2.5	1,188	1.0	0.010	-2—3
176	0.73	2.0	1.30	2.5	1,187	1.0	0.009	-2—3
Configuration -B2C1W1V1T05S1F1I1								
187	0.40	5.7	0.60	1.0	614	1.0	0.015	-4—23
188	0.40	5.7	0.80	1.4	723	1.0	0.012	-4—15
189	0.40	5.7	0.95	1.7	822	1.0	0.010	-1—8
190	0.40	5.7	1.05	1.9	849	1.0	0.010	0,2,4
191	0.40	5.7	1.20	2.1	983	1.0	0.010	0—5
192	0.40	5.7	0.30	1.0	1,112	1.0	0.029	-4—14

Table 4. Continued
a. Concluded

Run	d_s/d	l_s/d	M	$Re \times 10^{-6}$, ft $^{-1}$	P_t , psfa	θ , deg	$wd/2V$, radian	α , deg
Configuration -B2C1W1V1T05S1F1I1								
193	0.40	5.7	0.30	1.0	1,112	1.0	0.029	0 → 20
195	0.40	5.7	0.80	1.4	729	1.0	0.012	10, 12, 14
Configuration +B1C1W1V1T00S1F1I1								
203	0.65	5.6	0.30	2.5	3,012	1.0	0.030	0, -4
205	0.65	5.6	0.30	2.5	2,961	1.0	0.030	-4 → 15
206	0.65	5.6	0.95	1.0	485	1.0	0.015	-4 → 14
207	0.65	5.6	1.10	2.5	1,187	1.0	0.010	-2 → 3
208	0.65	5.6	1.30	2.5	1,188	1.0	0.009	0, 3
212	0.65	3.0	0.60	2.5	1,570	1.0	0.015	0
213	0.65	3.0	0.95	1.0	492	1.0	0.010	0
214	0.65	3.0	1.10	2.5	1,197	1.0	0.010	0
215	0.65	3.0	1.30	2.5	1,174	1.0	0.009	0
218	0.65	2.0	0.60	2.5	1,583	1.0	0.015	0
219	0.65	2.0	0.95	1.0	490	1.0	0.010	0
220	0.65	2.0	1.10	2.5	1,190	1.0	0.010	0
221	0.65	2.0	1.30	2.5	1,185	1.0	0.009	0

Table 4. Continued
b. Yaw-Damping

Run .	d_s/d	t_s/d	M	$Re' \times 10^{-6}$, ft $^{-1}$	p_t' , psfa	θ , deg	$\omega d/2V$, radian	α , deg
Configuration -B2C1W1V1T05S1F1I1								
313	0.4	5.7	0.30	1.0	1,108	1.0	0.029	-4 → 14
316	0.4	5.7	0.60	1.0	627	1.0	0.015	-4 → 14
317	0.4	5.7	0.80	1.4	746	1.0	0.012	-4 → 14
318	0.4	5.7	0.95	1.7	846	1.0	0.010	-4 → 14
319	0.4	5.7	0.95	1.7	843	1.0	0.010	0
320	0.4	5.7	1.05	1.8	883	1.0	0.009	-4 → 15
322	0.4	5.7	1.20	2.1	1,007	1.0	0.009	-4 → 15
323	0.4	5.7	1.20	2.1	1,009	1.0	0.009	0
Configuration -B1C1W1V1T05S1F1I1								
333	0.4	6.0	0.30	2.5	2,926	1.0	0.030	-4 → 25
335	0.4	6.0	0.60	2.5	1,622	1.0	0.016	-4 → 18
338	0.4	6.0	0.60	2.5	1,617	1.5	0.016	0
339	0.4	6.0	0.60	2.5	1,619	2.0	0.016	0
341	0.4	6.0	0.95	1.5	754	1.0	0.011	-4 → 14
342	0.4	6.0	0.95	1.5	748	1.5	0.011	0
343	0.4	6.0	0.95	1.5	748	2.0	0.011	0
344	0.4	6.0	0.95	1.5	753	1.0	0.011	0 → 12
346	0.4	6.0	1.10	2.5	1,230	1.0	0.010	-4 → 4
353	0.4	6.0	1.10	2.5	1,218	1.0	0.010	9 → 15
355	0.4	6.0	1.30	2.5	1,217	1.0	0.009	-4 → 15
360	0.4	4.0	0.60	2.5	1,600	1.0	0.015	0
362	0.4	4.0	0.95	1.5	735	1.0	0.010	0
370	0.4	2.0	0.60	2.5	1,605	1.0	0.015	0 → 15
372	0.4	2.0	0.95	1.5	752	1.0	0.010	0 → 15
374	0.4	2.0	1.10	2.5	1,215	1.0	0.010	0 → 15
376	0.4	2.0	1.30	2.5	1,202	1.0	0.008	0 → 15
380	0.4	3.0	0.60	2.5	1,597	1.0	0.015	0 → 15
382	0.4	3.0	0.95	1.5	757	1.0	0.010	0 → 15
384	0.4	3.0	1.10	2.5	1,207	1.0	0.010	0 → 15
386	0.4	3.0	1.30	2.5	1,217	1.0	0.008	0 → 15
390	0.65	4.0	0.60	2.5	1,595	1.0	0.015	0 → 14
391	0.65	4.0	0.60	2.5	1,595	1.0	0.015	0
392	0.65	4.0	0.95	1.5	749	1.0	0.010	0 → 14
394	0.65	4.0	1.10	2.5	1,204	1.0	0.010	0 → 15

Table 4. Concluded
b. Concluded

Run	d_s/d	l_s/d	M	$Re \times 10^{-6}$, ft $^{-1}$	p_t , psfa	θ , deg	$\omega d/2V$, radian	α , deg
Configuration -B1C1W1V1T05S1F1I1								
396	0.65	4.0	1.30	2.5	1,212	1.0	0.008	0 → 14
400	0.65	2.0	0.60	2.5	1,593	1.0	0.015	0 → 14
402	0.65	2.0	0.95	1.5	756	1.0	0.010	0 → 14
404	0.65	2.0	1.10	2.5	1,221	1.0	0.010	0 → 15
406	0.65	2.0	1.30	2.5	1,217	1.0	0.008	0 → 14
410	0.65	3.1	0.60	2.5	1,259	1.0	0.015	0 → 14
411	0.65	3.1	0.60	2.5	1,259	1.0	0.015	0
412	0.65	3.1	0.95	1.5	746	1.0	0.010	0 → 14
414	0.65	3.1	1.10	2.5	1,217	1.0	0.010	0 → 15
416	0.65	3.1	1.30	2.5	1,208	1.0	0.009	0 → 14
421	0.65	5.6	0.60	2.5	1,619	1.0	0.016	0 → 14
423	0.65	5.6	0.95	1.5	740	1.0	0.011	0 → 14
425	0.65	5.6	1.10	2.5	1,217	1.0	0.010	0 → 8
427	0.65	5.6	1.30	2.5	1,210	1.0	0.009	0 → 14
429	0.65	5.6	0.30	2.5	2,967	1.0	0.030	0
431	0.65	1.0	0.60	2.5	1,610	1.0	0.016	0
433	0.65	1.0	0.95	1.5	768	1.0	0.011	0
435	0.65	1.0	1.10	2.5	1,223	1.0	0.010	0
437	0.65	1.0	1.30	2.5	1,216	1.0	0.009	0

Table 5. Estimated Uncertainties
a. Basic steady-state measurements

Parameter Designation	STEADY-STATE ESTIMATED MEASUREMENT*							Range	Type of Measuring Device	Type of Recording Device	Method of System Calibration				
	Precision Index (S)			Bias (B)		Uncertainty $\pm(B + t_{958})$									
	Percent of Reading	Unit of Measurement	Degree of Freedom	Percent of Reading	Unit of Measurement	Percent of Reading	Unit of Measurement								
p_t , psfa	$\pm(0.04\% + 0.15)$	30		$\pm(0.11\% + 1)$		$\pm(0.2\% + 1.3)$		0 to 1,500	Datametrics Barocell Model 538AX-93; 0 - 4,000 psfa	Datametrics Electronic Manometer C-1018	In-place calibration with a precision pressure standard				
	—	± 0.7	30	—	± 2.9	—	± 4.3	1,500 to 4,000							
T_t , °R	—	± 0.1	6	—	± 0.55	—	± 0.77	410 to 610	Dual Chromel® - Alumel® Thermocouples	Newport Model 2600KF Digital Thermometer	Voltage standard substitution using a stirred ice bath thermocouple reference				
p_b , psfa	—	± 1.0	32	$\pm(0.14\% + 1)$		$\pm(0.14\% + 3)$		0 to 2,160	Sunstrand (Kistler) 314D Servo pressure Transducer	Preston Amplifier used with a Preston G-MAD-3 for A/D Conversion	In-place calibration with a precision pressure standard				
Tunnel sector pitch angle, deg	$\pm(0.014\% + 0.004)$	7	—	± 0.029		$\pm 0.03\% + 0.038$		-8 to 27	Clifton Precision products Model CG-10-AS-1 SYNCHRO Transmitter	Theta Model C-5280 Digital Indicator	In-place calibration by comparison to an inclinometer				
Tunnel sector roll angle, deg	—	± 0.04	7	—	± 0.300	—	± 0.390	±180							
Frequency, Hz	0.0025	—	2	—	0	0.01	—	0 to 10	A/D Frequency Converter Built by VKF	Digital Data Acquisition System (DDAS)	Compared with a frequency standard				

*Abernethy, R. B. et al. (Pratt and Whitney) and Thompson, J. W. (ARO, Inc.). "Handbook - Uncertainty in Gas Turbine Measurements." AEDC-TR-73-5 (AD 755356), February 1973.

Table 5. Continued

b. Basic dynamic measurements

Parameter Designation	STEADY-STATE ESTIMATED MEASUREMENT*								Range	Type of Measuring Device	Type of Recording Device	Method of System Calibration				
	Precision Index (S)		Bias (B)		Uncertainty $+(B + t_{95}S)$											
	Percent of Reading	Unit of Measurement	Degree of Freedom	Percent of Reading	Unit of Measurement	Percent of Reading	Unit of Measurement									
Out-of-Phase Torque, ft-lbs	0.87	---	>30	0.03	---	1.8	---	0 to 0.77	Bonded Strain Gages	Digital Data Acquisition System (DDAS)	In-place moment loading					
In-Phase Torque, ft-lbs	---	6.7×10^{-4}	>30	---	7.6×10^{-5}	---	0.0014	0 to 0.076								
In-Phase Sting Moment, ft-lbs	---	0.03	>30	---	0.06	---	0.12	0 to 16.5								
Out-of-Phase Sting Moment, ft-lbs	---	0.008	>30	---	0.008	---	0.024	0 to 0.4								
deg	0.4	---	>30	0.1	---	0.9	---	± 1 ± 2.5			Static loading					

*Abernethy, R. B. et al. (Pratt and Whitney) and Thompson, J. W. (ARO, Inc.). "Handbook - Uncertainty in Gas Turbine Measurements." AEDC-TR-73-5 (AD 755356), February 1973.

Table 5. Continued
c. Calculated parameters

Parameter Designation	STEADY-STATE ESTIMATED MEASUREMENT*							Parameter Range	Test Conditions		
	Precision Index (S)		Bias (B)		Uncertainty $\pm(B + t_{95}S)$						
	Percent of Reading	Unit of Measurement	Percent of Reading	Unit of Measurement	Percent of Reading	Unit of Measurement	M		$Re \times 10^{-6}$, ft^{-1}		
V, ft/sec	1.0		4.2		6.2	341	0.30	1.0			
	1.0		4.2		6.2	349	0.30	2.5			
	0.9		3.6		5.4	661	0.60	1.0			
	0.9		3.6		5.4	669	0.60	2.5			
	0.8		2.9		4.4	859	0.80	1.4			
	1.0		4.6		6.6	996	0.95	1.0			
	1.0		4.6		6.6	1,000	0.95	1.7			
	1.0		4.6		6.6	1,088	1.05	1.8			
	0.6		2.4		3.6	1,139	1.10	2.5			
	0.6		2.3		3.5	1,216	1.20	2.1			
	0.5		2.3		3.4	1,297	1.30	2.5			
Re, ft^{-1}	7,020		28,800		42,900	1.0	0.30	—			
	7,020		28,800		42,900	2.5	0.30	—			
	3,130		12,100		18,400	1.0	0.60	—			
	3,130		12,100		18,400	2.5	0.60	—			
	2,000		7,360		11,400	1.4	0.80	—			
	880		3,920		5,690	1.0	0.95	—			
	880		3,920		5,690	1.7	0.95	—			
	880		3,920		5,690	1.8	1.05	—			
	1,360		5,040		7,760	2.5	1.10	—			
	1,320		4,860		7,490	2.1	1.20	—			
	1,330		4,920		7,580	2.5	1.30	—			
q, psf	0.96		3.9		5.8	66	0.30	1.0			
	0.96		3.9		5.8	174	0.30	2.5			
	0.80		3.1		4.7	121	0.60	1.0			
	0.80		3.1		4.7	313	0.60	2.5			
	0.61		2.3		3.5	212	0.80	1.4			
	0.28		1.3		1.8	172	0.95	1.0			
	0.28		1.3		1.8	291	0.95	1.7			
	0.28		1.3		1.8	326	1.05	1.8			
	0.40		1.5		2.3	472	1.10	2.5			
	0.35		1.3		2.0	409	1.20	2.1			
	0.31		1.1		1.8	506	1.30	2.5			

*Abernethy, R. B. et al. (Pratt and Whitney) and Thompson, J. W. (ARO, Inc.). "Handbook - Uncertainty in Gas Turbine Measurements." AEDC-TR-73-5 (AD 755356), February 1973.

**In millions.

Table 5. Continued
c. Continued

Parameter Designation	STEADY-STATE ESTIMATED MEASUREMENT*						Parameter Range	Test Conditions		
	Precision Index (S)		Bias (B)		Uncertainty $\pm(B + t_{95}S)$					
	Percent of Reading	Unit of Measurement	Percent of Reading	Unit of Measurement	Percent of Reading	Unit of Measurement		M	$Re \times 10^{-6}$, ft ⁻¹	
p, psf	0.71		2.9		4.3	1,045	0.30	1.0		
	0.71		2.9		4.3	2,760	0.30	2.5		
	0.66		2.4		3.7	482	0.60	1.0		
	0.66		2.4		3.7	1,244	0.60	2.5		
	0.52		2.0		3.0	475	0.80	1.4		
	0.30		1.3		1.9	279	0.95	1.0		
	0.30		1.3		1.9	461	0.95	1.7		
	0.30		1.3		1.9	424	1.05	1.8		
	0.40		1.6		2.4	559	1.10	2.5		
	0.38		1.6		2.3	405	1.20	2.1		
	0.35		1.5		2.2	429	1.30	2.5		
M	0.0009		0.004		0.005	0.3	---	1.0		
	0.0009		0.004		0.005	0.3	---	2.5		
	0.0009		0.003		0.005	0.6	---	1.0		
	0.0009		0.003		0.005	0.6	---	2.5		
	0.0008		0.003		0.005	0.8	---	1.4		
	0.0011		0.005		0.007	0.95	---	1.0		
	0.0011		0.005		0.007	0.95	---	1.7		
	0.0011		0.005		0.007	1.05	---	1.8		
	0.0007		0.003		0.004	1.1	---	2.5		
	0.0007		0.003		0.004	1.2	---	2.1		
	0.0007		0.003		0.004	1.3	---	2.5		
<u>a, deg</u>	0.030	—	0.040	—	0.100	-4-24	—	—		

*Abernethy, R. B. et al. (Pratt and Whitney) and Thompson, J. W. (ARO, Inc.). "Handbook - Uncertainty in Gas Turbine Measurements." AEDC-TR-73-5 (AD 755356), February 1973.

Table 5. Continued
c. Continued

Parameter Designation	STEADY-STATE ESTIMATED MEASUREMENT*							Parameter Range	Test Conditions				
	Precision Index (S)		Bias (B)		Uncertainty $\pm(B + t_{95}S)$				M	$Re \times 10^{-6}$, ft ⁻¹	α , deg	$\omega d/2V$, radian	
	Percent of Reading	Unit of Measurement	Percent of Reading	Unit of Measurement	Percent of Reading	Unit of Measurement							
$C_{m_q} + C_{m_a}$, radian ⁻¹	0.062	---	0.085	---	0.210	-6.6	0.30	1.0	0	0.029			
	0.044	---	0.056	---	0.144	-4.6	0.30	2.5		0.030			
	0.071	---	0.058	---	0.200	-6.4	0.60	1.0		0.015			
	0.050	---	0.030	---	0.129	-4.8	0.60	2.5		0.015			
	0.095	---	0.059	---	0.249	-9.3	0.80	1.4		0.012			
	0.124	---	0.089	---	0.337	-12.7	0.95	1.0		0.011			
	0.146	---	0.087	---	0.380	-15.4	0.95	1.7		0.010			
	0.072	---	0.042	---	0.185	-7.2	1.05	1.8		0.010			
	0.046	---	0.018	---	0.110	-3.8	1.10	2.5		0.010			
	0.052	---	0.032	---	0.136	-6.1	1.20	2.1		0.010			
	0.047	---	0.020	---	0.114	-4.2	1.30	2.5		0.009			
C_{m_a} , radian ⁻¹	0.013	---	0.024	---	0.049	-0.40	0.30	1.0	0	0.029			
	0.006	---	0.006	---	0.018	0.27	0.30	2.5		0.030			
	0.008	---	0.014	---	0.030	-0.54	0.60	1.0		0.015			
	0.004	---	0.003	---	0.012	0.34	0.60	2.5		0.015			
	0.002	---	0.003	---	0.006	-0.24	0.80	1.4		0.012			
	0.006	---	0.002	---	0.014	0.07	0.95	1.0		0.011			
	0.007	---	0.004	---	0.018	-0.90	0.95	1.7		0.010			
	0.009	---	0.007	---	0.026	-1.68	1.05	1.8		0.010			
	0.007	---	0.004	---	0.017	-1.02	1.10	2.5		0.010			
	0.010	---	0.007	---	0.028	-1.97	1.20	2.1		0.010			
	0.006	---	0.003	---	0.016	-1.04	1.30	2.5		0.009			
C_m	0.0019	---	0.0070	---	0.0104	-0.117	0.30	1.0	20				
	0.0003	---	0.0004	---	0.0010	-0.049	0.30	2.5	14				
	0.0018	---	0.0050	---	0.0089	-0.204	0.60	1.0	24				
	0.0005	---	0.0008	---	0.0017	0.074	0.60	2.5	14				
	0.0008	---	0.0012	---	0.0028	-0.116	0.80	1.4	16				
	0.0004	---	0.0004	---	0.0012	-0.057	0.95	1.0	14				
	0.0004	---	0.0003	---	0.0012	-0.067	0.95	1.7	8				
	0.0001	---	0.0001	---	0.0004	-0.021	1.05	1.8	4				
	0.0004	---	0.0002	---	0.0009	-0.058	1.10	2.5	4				
	0.0005	---	0.0003	---	0.0012	-0.074	1.20	2.1	6				
	0.0003	---	0.0002	---	0.0008	-0.051	1.30	2.5	4				

*Abernethy, R. B. et al. (Pratt and Whitney) and Thompson, J. W. (ARO, Inc.). "Handbook - Uncertainty in Gas Turbine Measurements." AEDC-TR-73-5 (AD 755356), February 1973.

Table 5. Continued
c. Continued

Parameter Designation	STEADY-STATE ESTIMATED MEASUREMENT*						Test Conditions			
	Precision Index (S)	Bias (B)		Uncertainty $\pm(B + t_{95}S)$		Parameter Range	M	$Re \times 10^{-6}$, ft $^{-1}$	α , deg	$\omega d/2V$, radian
		Percent of Reading	Unit of Measurement	Percent of Reading	Unit of Measurement					
$c_{n_r} - c_{n_\beta} \cos \alpha$, radian $^{-1}$	0.0055		0.0074	0.0184	-0.57	0.30	1.0	0	0.076	
	0.0038		0.0052	0.0128	-0.43	0.30	2.5	0.080	0.040	
	0.0060		0.0061	0.0181	-0.70	0.60	1.0	0.042	0.031	
	0.0041		0.0030	0.0112	-0.50	0.60	2.5	0.028	0.027	
	0.0068		0.0050	0.0186	-0.78	0.80	1.4	0.025	0.024	
	0.0050		0.0036	0.0136	-0.63	0.95	1.5	0.027	0.023	
	0.0071		0.0045	0.0187	-0.82	0.95	1.7	0.029	0.029	
	0.0064		0.0038	0.0166	-0.75	1.05	1.8	0.027	0.027	
	0.0029		0.0017	0.0075	-0.40	1.10	2.5	0.024	0.024	
	0.0058		0.0035	0.0151	-0.69	1.20	2.1	0.023	0.023	
	0.0048		0.0027	0.0123	-0.62	1.30	2.5	0.023	0.023	
$c_{n_\beta} \cos \alpha$, radian $^{-1}$	0.005		0.014	0.027	0.24	0.30	1.0	0	0.080	
	0.002		0.003	0.006	0.11	0.30	2.5	0.080	0.040	
	0.003		0.005	0.011	0.21	0.60	1.0	0.042	0.031	
	0.001		0.001	0.003	0.10	0.60	2.5	0.028	0.027	
	0.002		0.002	0.006	0.23	0.80	1.4	0.025	0.025	
	0.002		0.001	0.005	0.19	0.95	1.5	0.027	0.027	
	0.002		0.002	0.006	0.36	0.95	1.7	0.024	0.024	
	0.002		0.001	0.006	0.35	1.05	1.8	0.023	0.023	
	0.002		0.002	0.005	0.32	1.10	2.5	0.023	0.023	
	0.002		0.001	0.007	0.48	1.20	2.1	0.024	0.024	
	0.002		0.0009	0.004	0.28	1.30	2.5	0.023	0.023	

*Abernethy, R. B. et al. (Pratt and Whitney) and Thompson, J. W. (ARO, Inc.). "Handbook - Uncertainty in Gas Turbine Measurements." AEDC-TR-73-5 (AD 755356), February 1973.

Table 5. Concluded
c. Concluded

Parameter Designation	STEADY-STATE ESTIMATED MEASUREMENT*						Parameter Range	Test Conditions		
	Precision Index (S)		Bias (B)		Uncertainty $\pm(B + t_{95}S)$					
	Percent of Reading	Unit of Measurement	Percent of Reading	Unit of Measurement	Percent of Reading	Unit of Measurement		M	$Re \times 10^{-6} \text{ ft}^{-1}$	
$\omega_d/2V$, radian (pitch)	8.7x10 ⁻⁵	8.7x10 ⁻⁵	3.6x10 ⁻⁴	5.3x10 ⁻⁴	2.9x10 ⁻²	0.30	1.0			
	8.7x10 ⁻⁵	8.7x10 ⁻⁵	3.6x10 ⁻⁴	5.3x10 ⁻⁴	3.0x10 ⁻²	0.30	2.5			
	2.1x10 ⁻⁵	3.2x10 ⁻⁵	1.2x10 ⁻⁴	1.5x10 ⁻²	0.60	1.0				
	2.1x10 ⁻⁵	3.1x10 ⁻⁵	1.2x10 ⁻⁴	1.5x10 ⁻²	0.60	2.5				
	1.1x10 ⁻⁵	4.0x10 ⁻⁵	6.1x10 ⁻⁵	1.2x10 ⁻²	0.80	1.4				
	1.1x10 ⁻⁵	4.8x10 ⁻⁵	6.9x10 ⁻⁵	1.0x10 ⁻²	0.95	1.0				
	1.1x10 ⁻⁵	4.7x10 ⁻⁵	6.9x10 ⁻⁵	1.0x10 ⁻²	0.95	1.7				
	9.7x10 ⁻⁶	4.3x10 ⁻⁵	6.2x10 ⁻⁵	1.0x10 ⁻²	1.05	1.8				
	5.4x10 ⁻⁶	2.2x10 ⁻⁵	3.3x10 ⁻⁵	1.0x10 ⁻²	1.10	2.5				
	4.5x10 ⁻⁶	1.8x10 ⁻⁵	2.8x10 ⁻⁵	9.7x10 ⁻³	1.20	2.1				
	3.9x10 ⁻⁶	1.6x10 ⁻⁵	2.4x10 ⁻⁵	9.2x10 ⁻³	1.30	2.5				
$\omega_d/2V$, radian (yaw)	2.3x10 ⁻⁴	9.3x10 ⁻⁴	1.4x10 ⁻³	7.6x10 ⁻²	0.30	1.0				
	2.3x10 ⁻⁴	9.6x10 ⁻⁴	1.4x10 ⁻³	8.0x10 ⁻²	0.30	2.5				
	5.5x10 ⁻⁵	2.1x10 ⁻⁴	3.2x10 ⁻⁴	3.9x10 ⁻²	0.60	1.0				
	5.8x10 ⁻⁵	2.2x10 ⁻⁴	3.4x10 ⁻⁴	4.2x10 ⁻²	0.60	2.5				
	2.7x10 ⁻⁵	1.0x10 ⁻⁴	1.6x10 ⁻⁴	3.1x10 ⁻²	0.80	1.4				
	2.8x10 ⁻⁵	1.3x10 ⁻⁴	1.8x10 ⁻⁴	2.8x10 ⁻²	0.95	1.5				
	2.8x10 ⁻⁵	1.2x10 ⁻⁴	1.8x10 ⁻⁴	2.7x10 ⁻²	0.95	1.7				
	1.4x10 ⁻⁵	5.5x10 ⁻⁵	8.2x10 ⁻⁵	2.5x10 ⁻²	1.05	1.8				
	1.4x10 ⁻⁵	5.6x10 ⁻⁵	8.4x10 ⁻⁵	2.7x10 ⁻²	1.10	2.5				
	1.1x10 ⁻⁶	4.5x10 ⁻⁵	6.7x10 ⁻⁵	2.4x10 ⁻²	1.20	2.1				
	9.8x10 ⁻⁶	4.1x10 ⁻⁵	6.0x10 ⁻⁵	2.3x10 ⁻²	1.30	2.5				

*Abernethy, R. B. et al. (Pratt and Whitney) and Thompson, J. W. (ARO, Inc.), "Handbook - Uncertainty in Gas Turbine Measurements," AEDC-TR-73-5 (AD 755356), February 1973.

APPENDIX

AERODYNAMIC CHARACTERISTICS OF THE SDM

The data presented in this section were obtained from two sources: (1) the present investigation, which is herein referred to as the dynamic test, and (2) previously unpublished static force and moment data obtained at AEDC, referred to as the static test. These data are presented in Figs. A-1 through A-3 and are compared with theoretical predictions (Ref. 10) where applicable. The data obtained during the dynamic test include C_m , $C_{m\alpha}$, $C_{n\beta} \cos \alpha$, $C_{m_q} + C_{m\alpha}$, $C_{n_l} - C_{n\beta} \cos \alpha$, and p_b/p , whereas during the static test, C_N , C_A , C_i , C_m , C_Y , and C_n data were obtained. Typical plots of the static test data are shown in Fig. A-1. A plot of C_m versus angle of attack (Fig. A-1d) shows good agreement between the data obtained from both the static and the dynamic tests. Comparison plots of C_m and $C_{m\alpha}$ versus Mach number (Fig. A-2) also show good agreement between the static and dynamic tests. Typical plots of data from the dynamic test are shown as functions of Mach number for two configurations (two different CG locations) in Fig. A-3 (pitch data) and Fig. A-4 (yaw data). For comparison with the SDM data, Fig. A-5 shows the base-pressure ratio variation with Mach number for the SDM and also shows base-pressure ratio data obtained for two slender conical models with and without a sting support. This comparison indicates that the SDM and the sting-supported cone have generally the same base-pressure trend.

At the beginning of the dynamic test, the variations of the parameters $C_{m_q} + C_{m\alpha}$, $C_{m\alpha}$, and p_b/p with unit Reynolds number were investigated at selected Mach numbers. These results are shown in Fig. A-6, and indicate no significant Reynolds number effects over the range investigated.

The effects of model oscillation amplitude (θ) on the pitch and yaw dynamic derivatives were also investigated, and are shown in Fig. A-7. The pitch dynamic derivatives showed a significant increase in dynamic stability due to amplitude at Mach numbers 0.95 and 1.10, and no effect at the other Mach numbers. This trend is reasonable, given the variation of the pitch dynamic derivatives with angle of attack at these Mach numbers (Ref. 5) and the definition of these parameters obtained by the forced-oscillation technique (local damping versus effective damping), which is outlined in detail in Ref. 11. No variation of the yaw dynamic derivatives with amplitude was found, though only Mach numbers 0.60 and 0.95 were investigated.

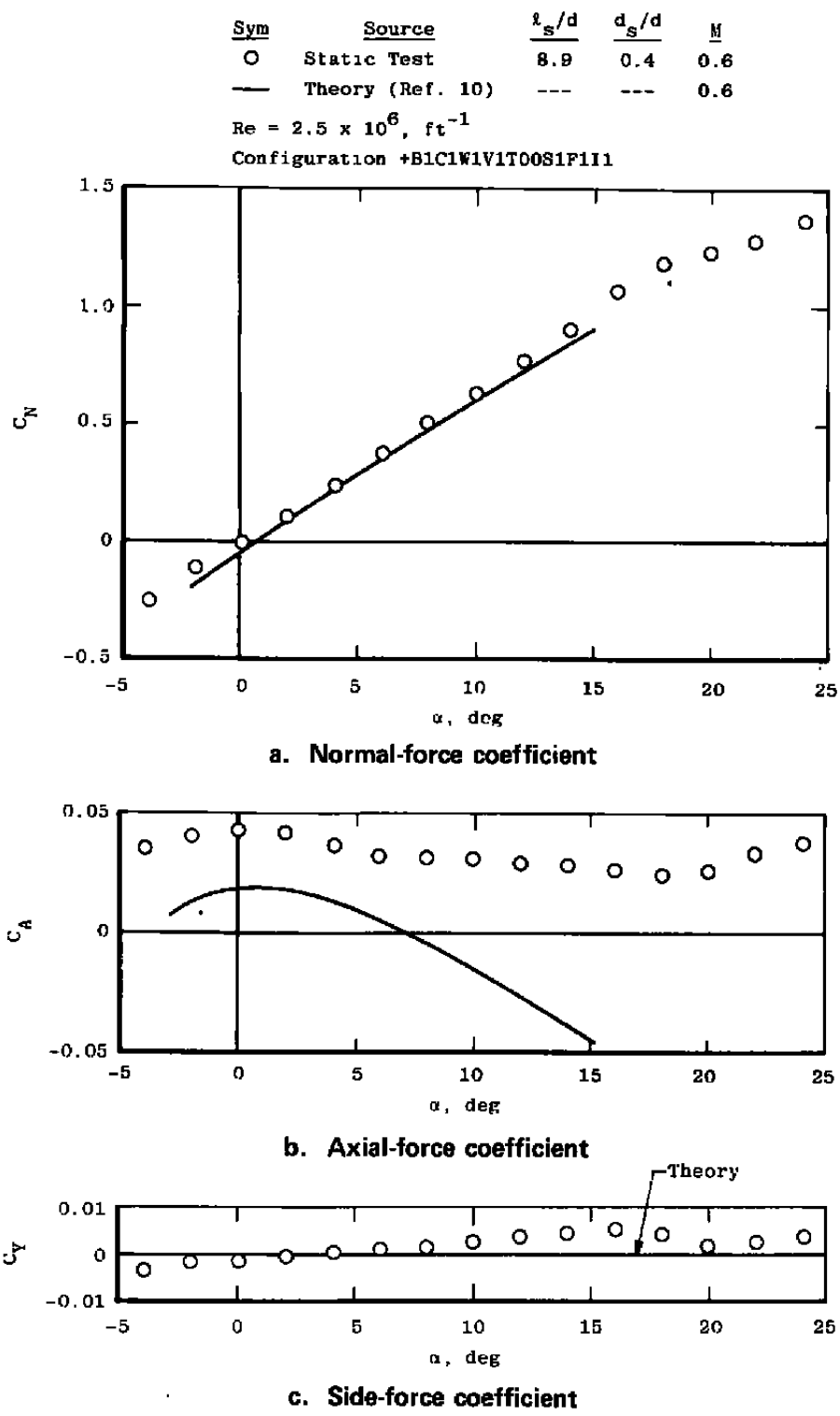
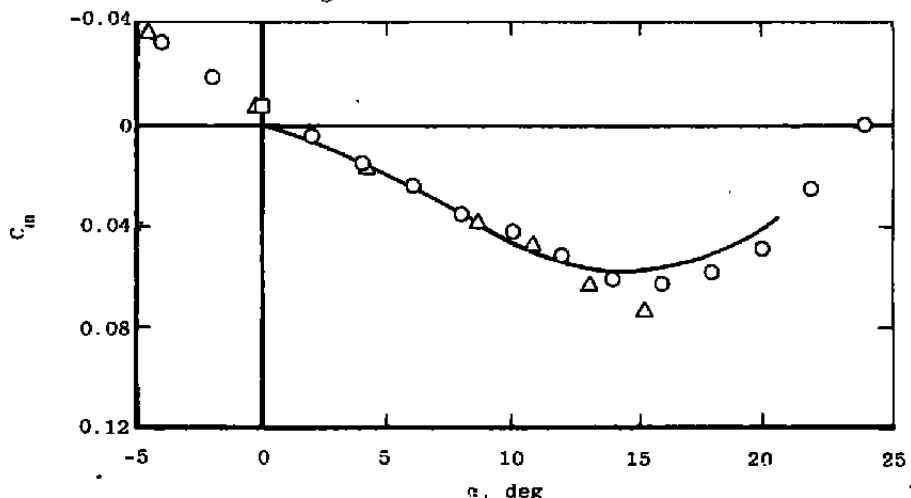


Figure A-1. Typical static force and moment measurements of the SDM.

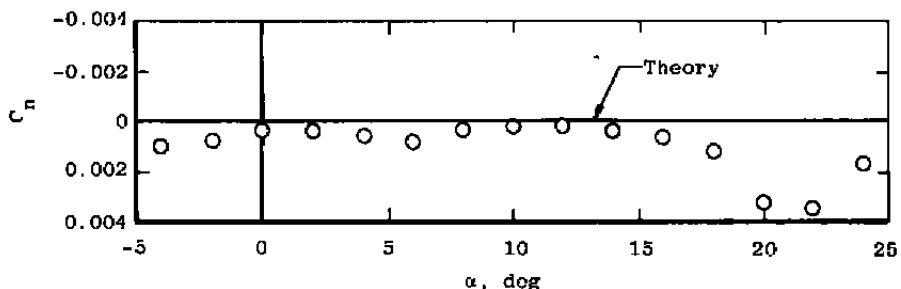
Sym	Source	$\frac{l_s}{d}$	$\frac{d_s}{d}$	M
○	Static Test	8.9	0.4	0.6
△	Dynamic Test	6.0	0.4	
—	Theory (Ref. 10)	---	---	

$Re = 2.5 \times 10^6$, ft $^{-1}$

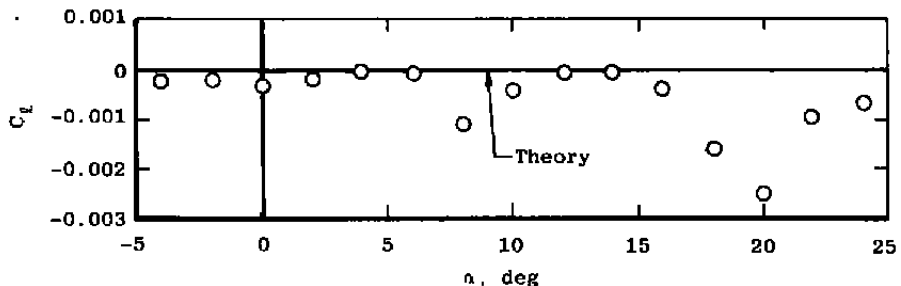
Configuration +B1C1W1V1T00S1F1I1



d. Pitching-moment coefficient



e. Yawing-moment coefficient



f. Rolling-moment coefficient

Figure A-1. Concluded.

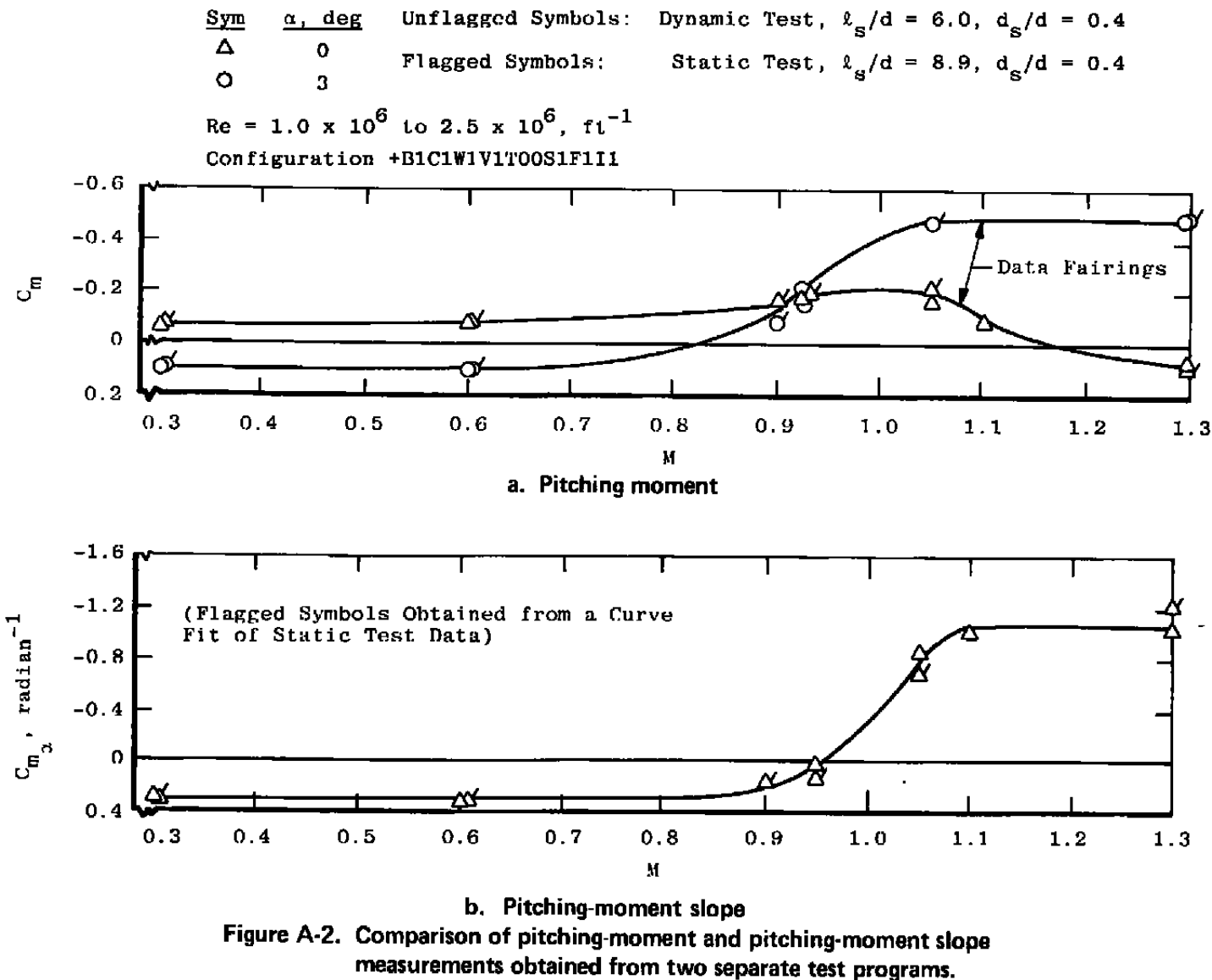
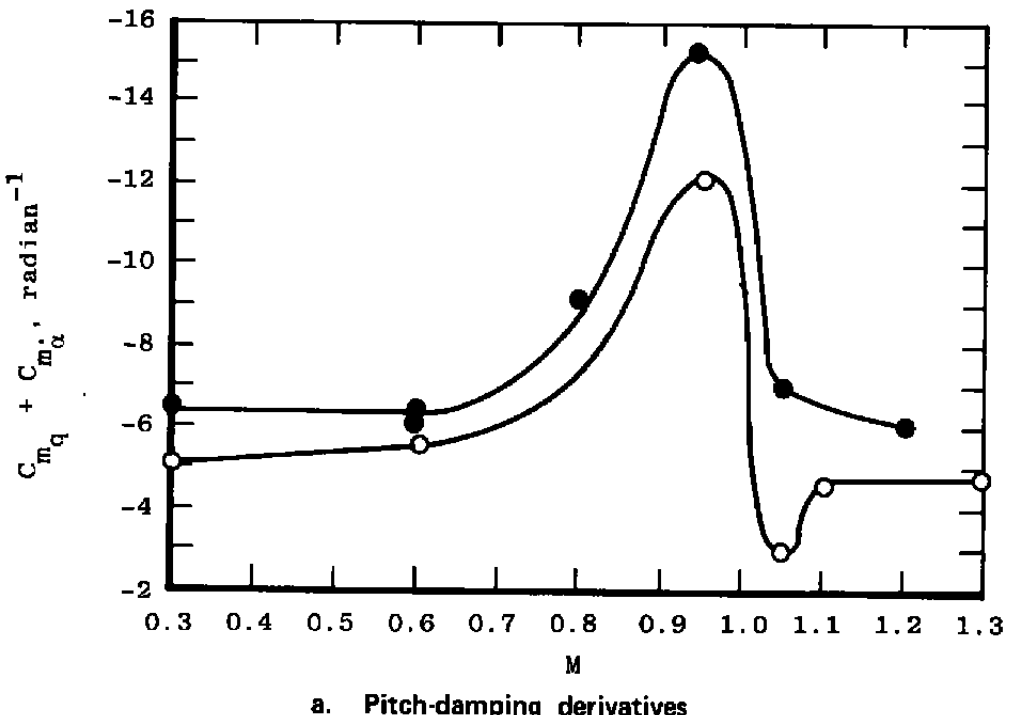


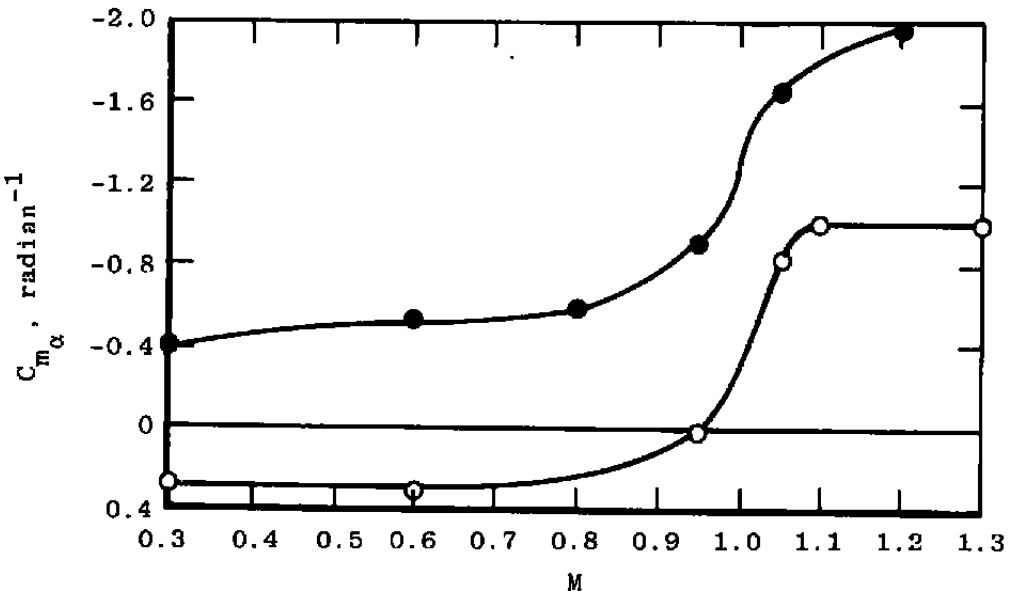
Figure A-2. Comparison of pitching-moment and pitching-moment slope measurements obtained from two separate test programs.

Sym	Configuration	$\frac{l_s}{d}$	$\frac{d_s}{d}$	θ , deg	α , deg
●	-B2C1W1V1T05S1F1II1	5.7	0.40	1.0	0
○	+B1C1W1V1T00S1F1II1	6.0	0.40	1.0	0

$Re = 1.0 \times 10^6$ to 2.5×10^6 , ft $^{-1}$



a. Pitch-damping derivatives



b. Pitching-moment slope

Figure A-3. SDM center-of-gravity effects on pitching-moment derivatives and variation with Mach number.

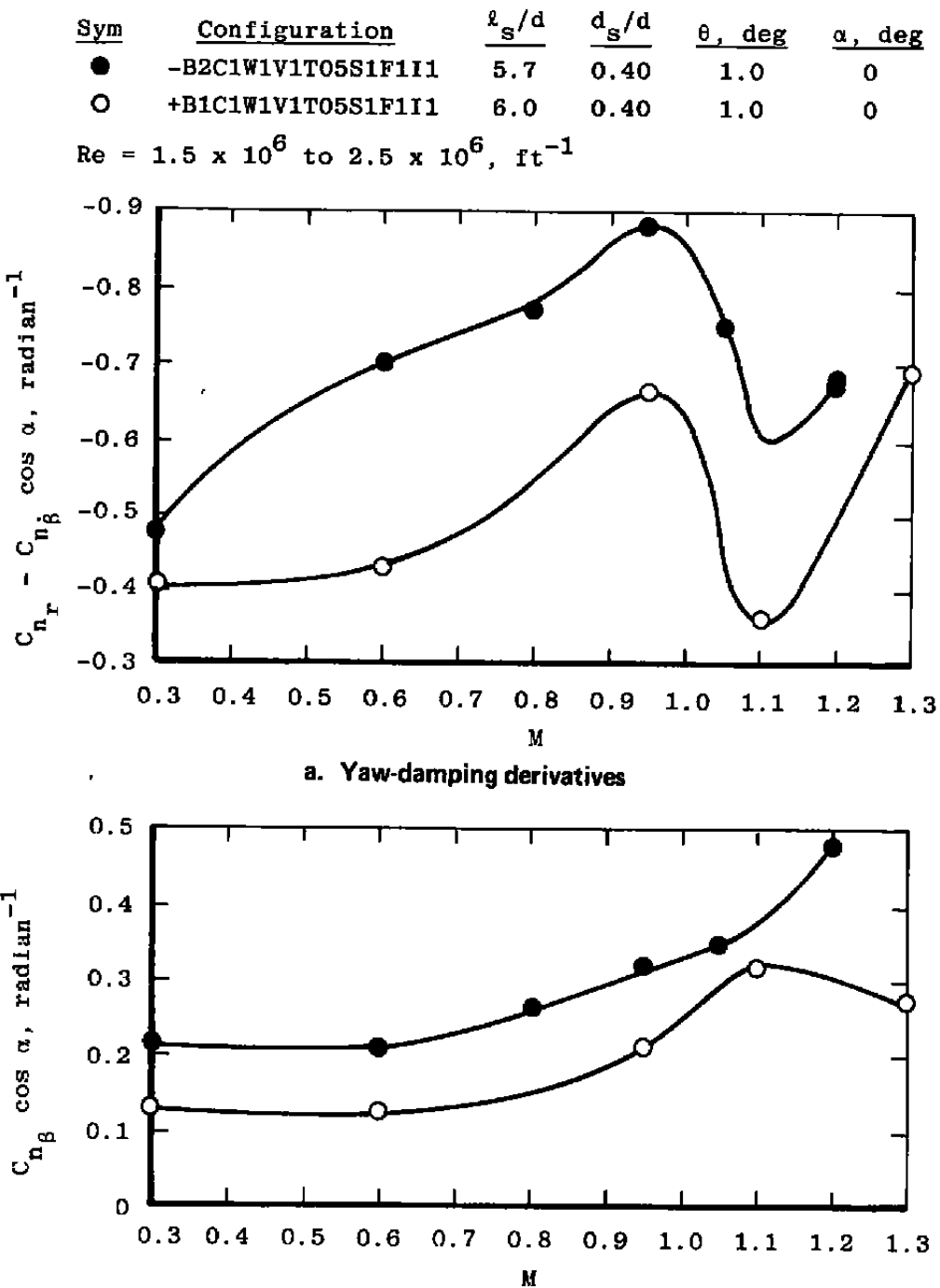


Figure A-4. SDM center-of-gravity effects on yawing-moment derivatives and variation with Mach number.

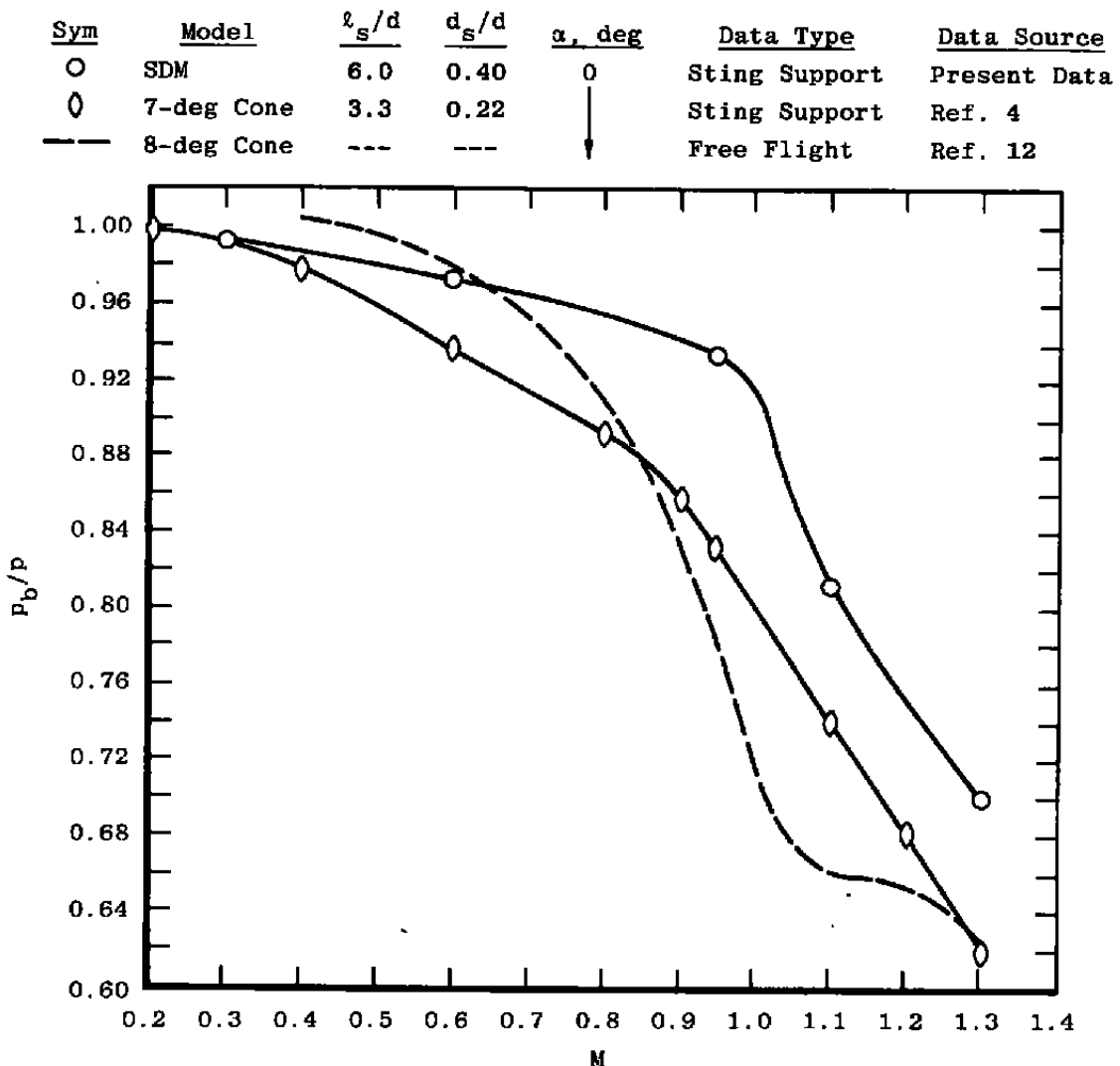


Figure A-5. Base-pressure ratio variation of the SDM with Mach number and comparison with other models.

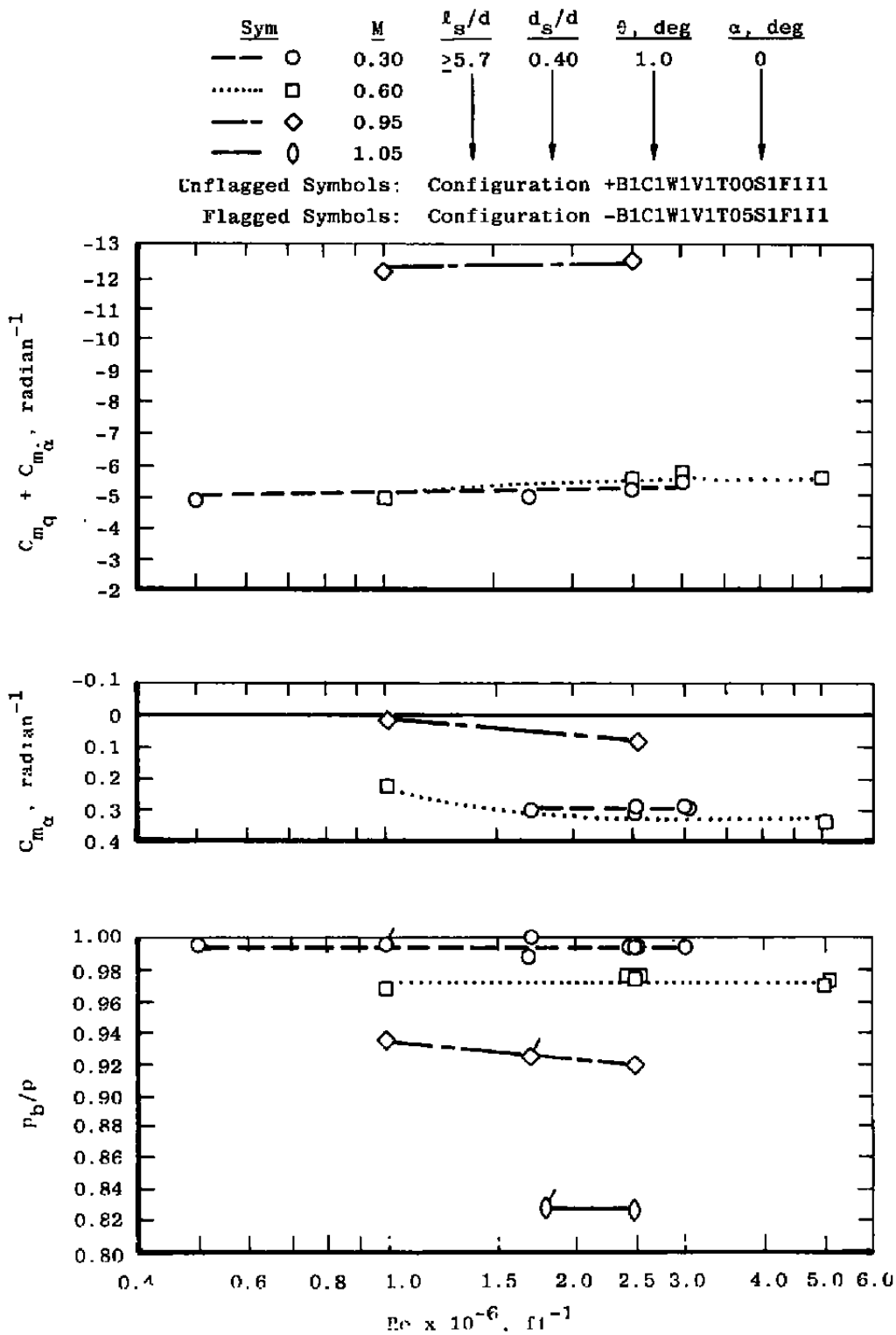


Figure A-6. Reynolds number effects on the SDM.

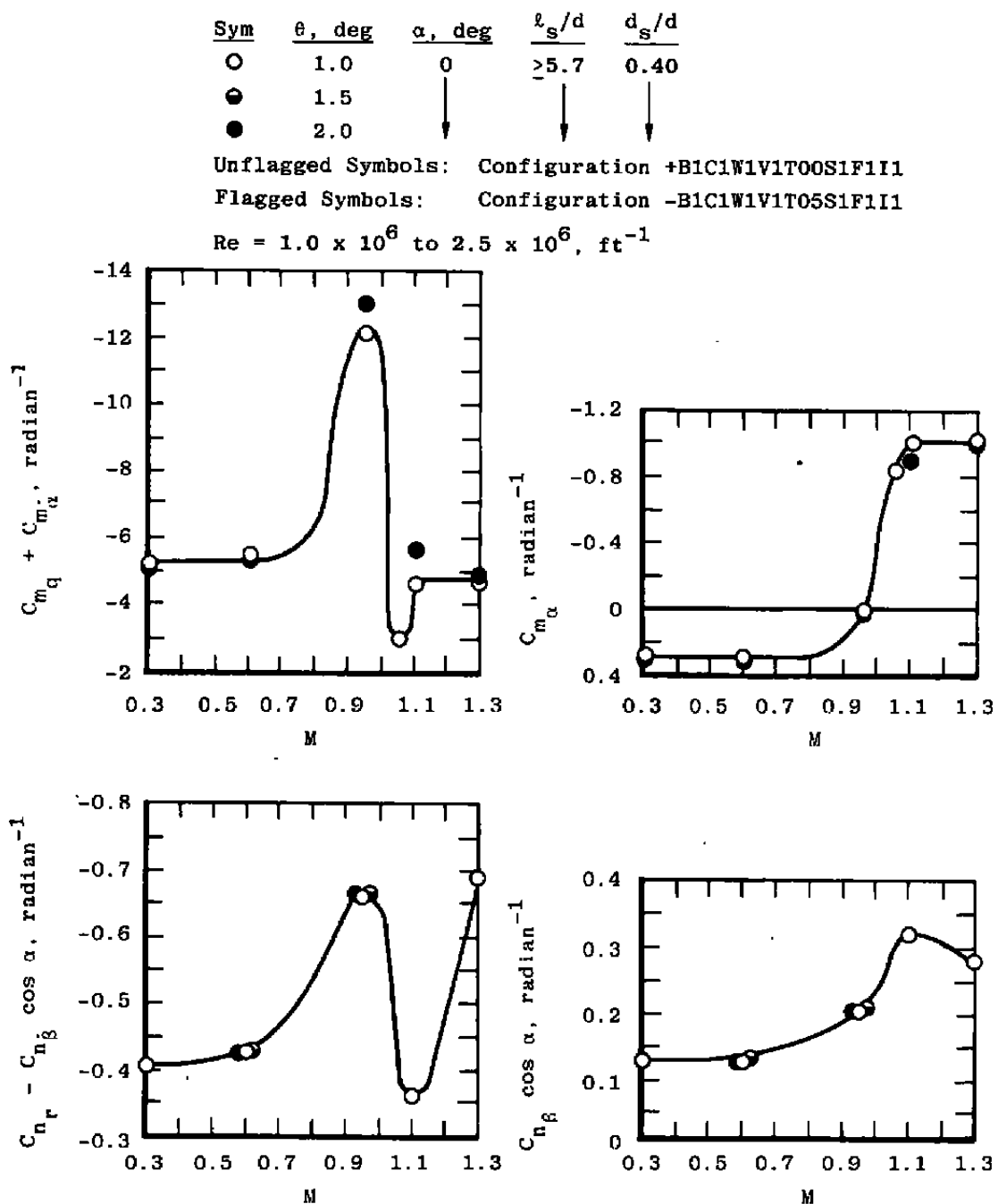


Figure A-7. Oscillation amplitude effects on the SDM.

NOMENCLATURE

A	Reference area (based on model planform wing area), 0.90702 ft ²
b	Model wing span, 1.65 ft
c	Model mean aerodynamic chord, 0.62233 ft
C_A	Axial-force coefficient, axial force/qA
CG	Center of gravity of model (see Table 1)
C_r	Rolling-moment coefficient, rolling moment/qAb
C_m	Pitching-moment coefficient, pitching moment/qA c
C_{m_q}	Pitching-moment coefficient due to pitch velocity, $\partial C_m / \partial (qc/2V)$, radian ⁻¹
C_{m_q} + C _{m_α}	Pitch-damping coefficient, radian ⁻¹
C_{m_α}	Pitching-moment coefficient due to angle of attack, $\partial C_m / \partial \alpha$, radian ⁻¹
C_{m_{α̇}}	Pitching-moment coefficient due to rate of change of angle of attack, $\partial(C_m) / \partial (\dot{\alpha}c/2V)$, radian ⁻¹
C_N	Normal-force coefficient, normal force/qA
C_n	Yawing-moment coefficient, yawing moment/qAb
C_{n_β} cos α	Yawing-moment coefficient due to angle of sideslip, $(\partial C_n / \partial \beta) \cos \alpha$, radian ⁻¹
C_n	Yawing-moment coefficient due to yaw velocity, $\partial(C_n) / \partial (rb/2V)$, radian ⁻¹
C_{n_r} - C _{n_β cos α}	Yaw-damping coefficient, radian ⁻¹
C_{n_β} cos α	Yawing-moment coefficient due to rate of change of sideslip, $[\partial(C_n) / \partial (\dot{\beta}b/2V)] \cos \alpha$, radian ⁻¹
C_y	Side-force coefficient, side force/qA
d	Reference length (model fuselage base diameter), 0.36458 ft
d_s	Effective sting diameter (at model base; see Figs. 3 and 4), ft
d_s/d	Sting diameter ratio

L. E.	Leading edge
l_{cr}	Critical sting length, in. (for $l_s < l_{cr}$, model data are affected)
l_{cr}/d	Critical sting length ratio
l_s	Effective sting length (from model base to sting flare; see Figs. 3 and 4)
l_s/d	Sting length ratio
F. S.	Model fuselage station (model nose = 0), in.
M	Free-stream Mach number
p	Free-stream static pressure, psf
p_b	Model base-pressure, psfa
p_b/p	Base-pressure ratio
p_t	Tunnel stilling chamber pressure, psfa
q	Pitching velocity, radian/sec, or free-stream dynamic pressure, psf
r	Yawing velocity, radian/sec
Re	Free-stream (unit) Reynolds number, ft^{-1}
Re_c	Free-stream Reynolds number based on model mean aerodynamic chord (\bar{c}), $Re_c = (Re/\text{ft})(\bar{c})$
T. E.	Trailing edge
T_t	Tunnel stilling chamber temperature, °R
V	Free-stream velocity, ft/sec
W.L.	Model waterline (model longitudinal centerline = 10.0), in.
α	Angle of attack, deg or radian
$\dot{\alpha}$	Time rate of change of angle of attack, radian/sec
β	Angle of sideslip, deg or radian
$\dot{\beta}$	Time rate of change of angle of sideslip, radian/sec
θ	Oscillation amplitude, 'deg
ω	Oscillation frequency, radian/sec
$\omega d/2V$	Reduced frequency parameter, $\omega \bar{c}/2V$ for pitch oscillation, and $\omega b/2V$ for yaw oscillation, radian

Abbreviations

A/D	Analog to digital converter
AMAPS	Automatic Model Attitude Positioning System
DDAS	Digital Data Acquisition System
OC	Oscillatory component of balance signal
SC	Static component of balance signal